Chemical Geology 641 (2023) 121780

Contents lists available at ScienceDirect

Chemical Geology

journal homepage: www.elsevier.com/locate/chemgeo

Petrogenesis of alkaline magmas across a continent to ocean transect, northern Ross Sea, Antarctica

K. Durkin [a], J.M.D. Day [a], K.S. Panter [b], J.-F. Xu [c], P.R. Castillo [a,*]

[a] Scripps Institution of Oceanography, University of California, San Diego, La Jolla, CA 92093, USA
[b] Bowling Green State University, Bowling Green, OH 43403, USA
[c] China University of Geosciences (Beijing), Beijing 100083, China

ARTICLE INFO

Editor: S Aulbach

Keywords:
Continent-ocean transition
Continental alkaline lavas
OIB-like lavas
Recycled oceanic lithosphere
FOZO
Osmium

ABSTRACT

The West Antarctic Rift System (WARS) is one of the world's largest active rift systems and alkaline magmatic provinces. The alkaline magmatism crosscuts oceanic and continental lithosphere but maintains generally similar Sr-Nd-Pb isotope signatures. Here we present new major-, trace- and highly siderophile-element (Os, Ir, Ru, Pt, Pd, Re) abundances and Sr-Nd-Pb-Os isotope data for a Miocene to recent WARS alkaline basalt suite from a continental-oceanic transect in the northwest Ross Sea. The samples are geochemically enriched similar to ocean island basalts, with oceanic lavas having higher absolute incompatible trace element abundances than continental lavas. The suite exhibits a large range in measured $^{187}Re/^{188}Os$ (1.7 to 1305) and age-corrected $^{187}Os/^{188}Os$ (0.1254 to 1.055) that has a positive, highly curved relationship with measured $^{87}Sr/^{86}Sr$ (0.70287–0.70331), but a negative, highly curved relationship with both measured $^{143}Nd/^{144}Nd$ (0.51280–0.51300) and $^{206}Pb/^{204}Pb$ (19.237–20.237). These data suggest that contamination by a mafic continental lithospheric component has occurred to varying degrees and exerts some control on the geochemistry of the continental lavas. Primitive lavas from the oceanic Adare Basin that have experienced negligible contamination are used to constrain the primary source of northwest Ross Sea alkaline lavas and to assess previously proposed hypotheses regarding the origin of magmatism. Explanations for the origin of WARS alkaline lavas range from plume magmatism to partial melting of continental lithospheric mantle metasomatized by subduction fluids prior to cessation of subduction of the Phoenix Plate underneath the Gondwana margin. Samples from the continental-oceanic transect, however, neither exhibit classic arc-lava geochemical signatures nor provide any evidence to support an active mantle plume source. Rather, they are geochemically enriched magmas generated through partial melting of previously subducted oceanic lithospheric mantle concomitant with continental lithospheric thinning during the Cenozoic.

1. Introduction

The West Antarctic Rift System (WARS; Fig. 1), one of the world's largest active rifts, underwent two primary periods of extension; an amagmatic period during the Cretaceous followed by a second extension phase during the Cenozoic (e.g., Davey and Brancolini, 1995; Salvini et al., 1997; Cande et al., 2000; Huerta and Harry, 2007; Ji et al., 2018). The second phase has been the subject of much discussion as it is accompanied by widespread alkaline volcanism, enabling assessment of magma sources and partial melting processes. This volcanism has traditionally been divided into the Hallett, Melbourne and Erebus volcanic provinces that all belong to the McMurdo Volcanic Group (Kyle et al., 1990; Smellie and Rocchi, 2021). Alkaline volcanism in the WARS is particularly remarkable as it occurs from the Antarctic continent in northern Victoria Land to the oceanic crust in the northwest Ross Sea region (Panter and Castillo, 2007; Aviado et al., 2015; Panter et al., 2018). Only two other locations in the world are known to host a continent-ocean transect of petrologically and geochemically related alkaline volcanoes. Magmatism in the East African Rift System, another large active rift, has also been found quite recently to extend to dome-like volcanic structures in the Mozambique Ridge in the Indian Ocean (O'Connor et al., 2019). A long established continent-ocean magmatic province is the Cameroon Volcanic line (e.g., Fitton and Dunlop, 1985; Ngwa et al., 2017). The origins of alkaline magmatism in both settings

* Corresponding author.
E-mail address: pcastillo@ucsd.edu (P.R. Castillo).

https://doi.org/10.1016/j.chemgeo.2023.121780
Received 7 August 2023; Received in revised form 10 October 2023; Accepted 10 October 2023
Available online 15 October 2023

remain enigmatic.

The continental to oceanic transition in the WARS has been sampled through field-based investigations and ship-based dredging operations (Panter and Castillo, 2007; Aviado et al., 2015; Panter et al., 2018). Samples from these studies have included lavas erupted onto continental crust (e.g., northern Victoria Land, Daniell and Adare peninsulas, and the Melbourne Volcanic Province) as well as forming islands in the Ross Sea (Coulman and Possession islands) and oceanic crust in the adjacent Adare Basin. Although not initially described as part of WARS, the Adare Basin likely represents a contiguous manifestation of Cenozoic extension since it is blanketed by a sequence of sedimentary strata that can be traced to the adjacent Ross Sea sedimentary basins, and overlies a set of magnetic anomalies striking NNW-SSE, generally orthogonal to the rift extensional direction (Cande and Stock, 2006; Davey et al., 2006). Previous studies have indicated that WARS volcanic rocks share similar geochemical signatures despite differences in the composition of crust that they pass through. Specifically, WARS samples are characterized by ocean island basalt (OIB)-like major and trace element compositions and their Sr-Nd-Pb isotope ratios are similar to OIB with a high μ (HIMU)-like isotopic signature (Hart et al., 1992; Panter et al., 2018; Panter and

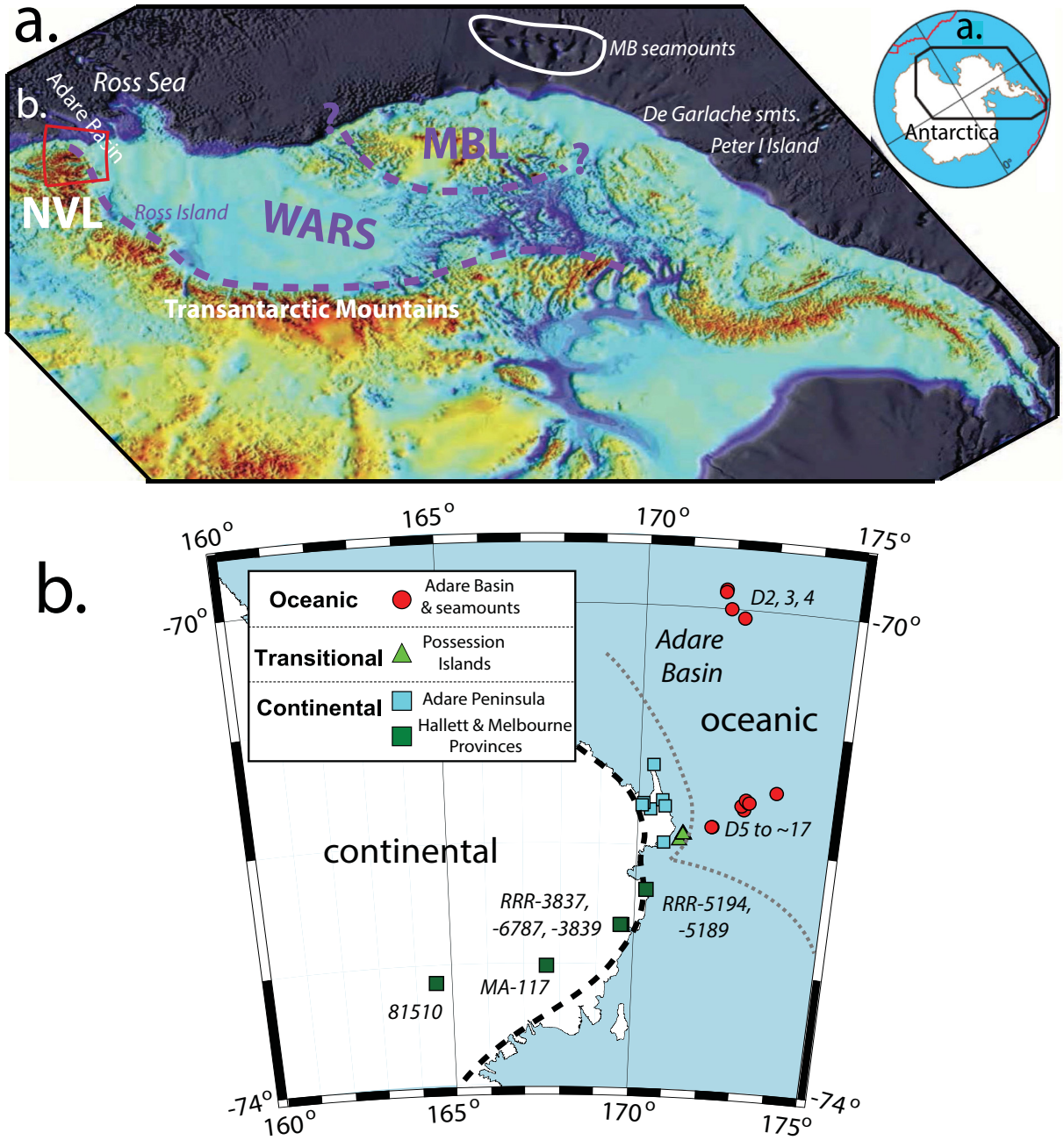

Fig. 1. Regional and sample location maps. a. Subglacial surface elevation map (after Panter et al., 2018) with the approximate boundaries of the West Antarctic Rift System (WARS) delimited by purple dashed lines. Also shown are locations of oceanic volcanic fields (seamounts and islands) that are compared in this study. NVL = Northern Victoria Land; MBL = Mary Byrd Land; MB seamounts = Marie Byrd seamounts. b. Regional map of the NW Ross Sea showing the approximate location of samples from Adare Basin (red circles) in the oceanic setting, Possession Islands (green triangles) in the ocean-continent transition region and Adare Peninsula (cyan squares) and Hallett and Melbourne volcanic fields (dark green squares) in the continental setting. Sample numbers for the oceanic Adare Basin and seamounts and continental Hallett and Melbourne volcanic provinces are shown (Adare Peninsula and Possession Islands samples are too close to one another). Data from this study and Panter et al. (2018). (For interpretation of the references to colour in this figure legend, the reader is referred to the web version of this article.)

Martin, 2023). Unlike typical OIB and/or HIMU sensu stricto basalts with $^{206}Pb/^{204}Pb > 20.5$, however, these samples possess only moderate geochemical and isotopic enrichments similar to the vast majority of West Antarctic basalts; lavas with a HIMU-type signature are present at only few localities (Panter et al., 2000). Also, unlike many oceanic, plume-related HIMU basalt occurrences, the volcanism in the northern Ross Sea lacks a clear linear age progression and shows only a weak northward younging, from continental to oceanic crust (Panter and Castillo, 2007; Panter et al., 2018). The existence of contiguous alkaline volcanism crossing continental to oceanic lithosphere in the WARS presents two questions: (1) is this volcanism representative of a common magmatic source and mechanism for melting, and (2) can some of the differences in geochemical signatures between continental and oceanic regimes be accounted for by the interaction of a common magma with oceanic and continental lithosphere? Addressing these questions has ramifications for interpreting volcanic rocks erupted in continental and oceanic settings worldwide.

Previous work in the WARS has suggested several mechanisms to explain both the timing of volcanism as well as the geochemically enriched isotopic signatures observed in the alkaline volcanic rocks. One proposed mechanism for generating the alkaline volcanism is melting of a Cenozoic mantle plume under Mt. Erebus on Ross Island (Kyle et al., 1990; Sims et al., 2008; Phillips et al., 2018). Similarly, an older (Late Cretaceous) and larger mantle plume has been proposed to have controlled break-up of Zealandia from West Antarctica and the HIMU-type isotopic signature of mafic magmatism (e.g., Lanyon et al., 1993; Weaver et al., 1994; Storey et al., 1999). A proposed variant of this hypothesis has suggested that plumes underplated and accreted to the base of the Gondwana lithosphere prior to break-up, leading to a *fossil plume* source, which then was melted during Cenozoic extension (Rocholl et al., 1995; Hart et al., 1997; Panter et al., 2000; Kipf et al., 2014). The other proposed mechanisms can be collectively grouped as non-plume hypotheses, which argue that the controlling factor on the similar geochemical signatures of WARS alkaline basalts is the nature of continental lithospheric mantle (CLM). The CLM is suggested to have been metasomatized by subduction-related fluids (e.g., Finn et al., 2005; Aviado et al., 2015; Day et al., 2019), or by carbonate-rich melts from previously subducted oceanic slabs at the Gondwana margin (Panter et al., 2018). In these models, WARS magmas are generated from the metasomatized CLM during rifting or due to the influx of the convecting Pacific asthenosphere (e.g., Finn et al., 2005; Faccenna et al., 2008; Nardini et al., 2009; Panter, 2021).

In this study, samples from a continental-oceanic transect in the western Ross Sea embayment (Fig. 1) were analyzed to constrain the source and petrogenesis of WARS alkaline magmatism. Continental samples are from the Adare Peninsula and both the Hallett and Melbourne volcanic provinces (Adare, Hallett and Daniell peninsula volcanic fields and Mt. Overlord and Malta Plateau volcanic fields that altogether are herein abbreviated HMp), continent-ocean transition samples are from the Possession Islands and oceanic samples are from Adare Basin and seamounts (ABS). Many of these samples were previously analyzed for their major and trace element abundances and Sr-Nd-Pb isotopes (Panter and Castillo, 2007; Panter et al., 2018) to constrain the petrology and geochemistry of the alkaline lavas. In addition to these geochemical tracers, we present ^{187}Re—^{187}Os and highly siderophile element (HSE; Os, Ir, Ru, Pt, Pd, Re) abundance systematics in the previously analyzed and new samples. Since these latter elements are both siderophile and chalcophile, as well as generally strongly compatible, they complement the lithophile element abundance and isotope tracers. Osmium isotopes are sensitive tracers of both continental crustal contributions, which has highly radiogenic $^{187}Os/^{188}Os$ (typically >1) compared to mantle-derived melts (~0.129) and CLM (typically <0.125) (Day, 2013). The sensitivity of Os isotopes to contamination has recently been demonstrated during time-series measurements of recently erupted OIB (Day et al., 2022). This study therefore offers a new perspective by using combined Sr-Nd-Os-Pb isotopes, in conjunction with O isotope data reported previously (Panter et al., 2018), to more fully assess existing models for the petrogenesis of alkaline WARS magmas.

2. Geologic background

2.1. Tectonics

Northern Victoria Land is in the westernmost section of the East Antarctic Craton adjacent to the Ross Sea (Fig. 1). It is comprised of three continental litho-tectonic blocks fused during the Ross Orogeny in the Proterozoic as part of the larger Terra Australis orogen (Borg and Stump, 1987; Boger and Miller, 2004; Di Vincenzo et al., 2016). The Terra Australis orogen concluded with the formation of Pangaea and was followed by the Gondwanide orogeny in the Triassic as the Phoenix Plate subducted beneath the Gondwana margin (Cawood, 2005). Subduction ceased abruptly in the Cretaceous (Bradshaw, 1989). The mechanism of subduction cessation along this margin is still unresolved; oblique subduction of the Phoenix-Pacific spreading center (Bradshaw, 1989), slab capture (Luyendyk, 1995), collision with the Hikurangi Plateau (Davy et al., 2008), and plume upwelling (Hoernle et al., 2020) have all been suggested as methods by which this abrupt termination may have occurred. Subduction cessation in the Late Cretaceous marked a shift from a compressional to extensional tectonic regime that led to the formation of the WARS (Jordan et al., 2020 and references therein).

The resultant WARS is a region of thinned lithosphere that stretches from the Antarctic Peninsula to the Ross-Embayment-northern Victoria Land and separates West Antarctica from the East Antarctic Craton. The broadest part of the WARS, the Ross Sea, is comprised of a series of N-S oriented sedimentary basins (e.g., northern Victoria Land Basin, Northern Basin). The first stage of crustal extension in the region was an amagmatic lithospheric thinning that led to a 500–1000 km widening of the Ross Sea during the early Late Cretaceous (Davey and Brancolini, 1995; Salvini et al., 1997; Cande et al., 2000). The second phase was focused primarily in the western Ross Sea, near northern Victoria Land and formed the Transantarctic Mountains (Huerta and Harry, 2007; Ji et al., 2018). This phase further opened the Ross Sea by ~300 km and was accompanied by alkaline magmatism as well as increased heat flow (Risk and Hochstein, 1974) and low seismic shear wave velocities (Lawrence et al., 2006; Lloyd et al., 2020).

The Adare Basin lies immediately east of the Adare Peninsula, at the northern end of Ross Sea (Fig. 1). It was formed as an arm of a ridge-ridge-ridge triple junction that accommodated 140–170 km of ENE-WSW extension during Eocene-Oligocene time (Cande et al., 2000; Cande and Stock, 2006; Granot et al., 2013). All subsequent separations were accommodated by normal faulting, creating a rifting graben, the Adare Trough (Granot et al., 2010, 2013). The Adare Basin is defined by a set of magnetic anomalies that strike NNW-SSE which constrain its formation to 43–26 Ma (Cande et al., 2000). These magnetic anomalies extend into the Northern Basin, the closest continental basin, linking the Adare seafloor spreading to the extensional tectonics of the western Ross Sea (Cande and Stock, 2006; Davey et al., 2006). The Northern and Adare basins are further linked by a continuous Bouguer anomaly and contiguous sedimentary sequences (Cande and Stock, 2006; Davey et al., 2006). In general, the geologic evolution of the Adare Basin and adjacent western East Antarctica from continental block fusion, plate subduction associated with plate collision and, finally, subduction cessation leading to tectonic extension provides the backdrop for the continental-oceanic WARS magmatism.

2.2. Magmatism

The McMurdo Volcanic Group is part of the Western Ross Supergroup (Rocchi et al., 2002) of volcanism that stretches along the entire western boundary of the Ross Sea and greater WARS (Fig. 1). It is made up of Cenozoic basaltic shield volcanoes, trachytic or phonolitic

stratovolcanoes and scattered basaltic cinder cones, lava flows, and evolved lava domes (Smellie and Rocchi, 2021; Smellie and Martin, 2021). Although it is regionally subdivided into the Erebus, Melbourne, and Hallett volcanic provinces, the McMurdo Group as a whole can be described as distinctly silica-undersaturated and alkaline (Kyle et al., 1990; Panter, 2021).

The Melbourne Volcanic Province extends northward from Mount Melbourne to the south/southwestern boundary of the Hallett Volcanic Province and can be subdivided into four major volcanic fields (Malta Plateau, The Pleiades, Mount Overlord, and Mount Melbourne) with a series of small basaltic vents and lava flows that are located mainly in the Transantarctic Mountains (Smellie and Rocchi, 2021). Lava compositions range from alkali basalt and strongly Si-undersaturated basanite to peralkaline trachyte and rhyolite and rare phonolite (Rocchi and Smellie, 2021). The oldest lavas (c. 6–11 Ma) along with alkaline dikes (c. 12 Ma) are found on the Malta Plateau, while Mount Overlord is the oldest stratovolcano (c. 7–8 Ma) within the Melbourne Volcanic Province (Smellie and Rocchi, 2021).

Like the Melbourne Volcanic Province, the Hallett Volcanic Province consists of N-S elongated shield volcanoes that occur at the Adare, Hallett and Daniell peninsulas and Coulman Island volcanic fields. The Possession Islands are grouped within the Adare Peninsula Volcanic Field (Smellie and Rocchi, 2021). The province is composed predominantly of basanite, alkali basalt and hawaiite lavas although evolved compositions (e.g., trachyte, phonolite) exist at several locations (Rocchi and Smellie, 2021). Most of the volcanism ranges in age from c. 13 to 5 Ma (Smellie et al., 2011) with the Possession Islands being significantly younger (< 1 Ma; Panter et al., 2018; *Erratum*).

Additional volcanism, herein informally grouped with the Hallett Volcanic Province, is adjacent to and to the NE of the Adare Peninsula and covers an area of ~35,000 km^2 (Fig. 1). The submarine volcanism, initially identified based on seafloor bathymetry, consists of seamounts found on the continental shelf, within the Adare Basin and Adare Trough (Panter and Castillo, 2007). The mostly small volcanic centers exhibit a N-S orientation, similar to regional faulting and alignment of volcanism in the Hallett Volcanic Province (Panter and Castillo, 2007; Panter et al., 2018). Relative ages based on seismic stratigraphic relationships (Granot et al., 2010) indicate that these volcanic centers are contemporaneous and are likely to be a continuation of continental WARS volcanism. Dating of dredged seamount lavas by the $^{40}Ar/^{39}Ar$ method confirmed their young age (14 samples c. 4.6–0.14 Ma, with one sample dated at 15.9 ± 0.8 Ma; Panter et al., 2018; *Erratum*). Overall, there is a slight age-progression in volcanism during the Pliocene to Pleistocene from volcanic centers on the Daniell Peninsula NE to seamounts on the continental shelf and into the Adare Basin (Smellie et al., 2011; Panter et al., 2018).

3. Methods

Samples analyzed in this study consist of submarine lavas collected by dredging from the Adare Basin seamounts and crust during the US National Science Foundation funded NBP0710 expedition in the northern Ross Sea aboard the icebreaker RV/IB Nathaniel B. Palmer in the Austral summer of 2006–2007 (Panter and Castillo, 2007; Panter et al., 2018). Subaerial samples from the volcanic provinces were obtained from the Polar Rock Repository (PRR), Byrd Polar and Climate Research Center (http://research.bpcrc.osu.edu/rr/) and were collected during various prior field expeditions. The samples, including those used by Panter and co-workers (Panter and Castillo, 2007; Panter et al., 2018), were crushed in a tungsten carbide-lined jaw crusher into cm-sized fragments, examined to remove visibly altered chips, and powdered using a Spex alumina ceramic grinding container. Major element oxide and some trace element analyses were performed by X-ray fluorescence (XRF) spectrometry at the GeoAnalytical Laboratory of Washington State University (WSU) using the procedure described by Johnson et al. (1999). Trace elements were analyzed at the Scripps Isotope Geochemistry Laboratory (SIGL). For the analysis, 50 mg of sample powder was dissolved and analyzed using an iCAP Qc ICP-MS following standard analytical procedures outlined in Day et al. (2014). Data quality was monitored by repeated measurements of international standards (BHVO-2, BCR-2 and BIR-1) and total procedural blanks prepared with samples. Reproducibility of the major and trace elements of reference materials was generally better than 5% (RSD); precision was c. 2% for most major and c. 5% for most trace elements (see notes under Supplementary Table 1).

The same powders were also used for all Sr, Nd, and Pb isotope analyses, which were performed at Scripps Institution of Oceanography (SIO) according to methods described in Janney and Castillo (1996). Strontium and the rare earth elements (REE) were initially separated using cation-exchange columns and HCl as eluent. The REE cut underwent a second separation using hydroxyisobutyric acid as eluent to isolate Nd for isotope analyses. Lead separation was conducted using standard anion exchange methods in an HBr medium. All Pb-Sr-Nd isotope ratios were analyzed using a nine-collector, Micromass Sector 54 thermal ionization mass spectrometer (TIMS). Strontium isotopic ratios were fractionation-corrected to $^{86}Sr/^{88}Sr = 0.1194$ and are reported relative to $^{87}Sr/^{86}Sr = 0.710254 \pm 0.000018$ ($n = 22$) for NBS 987. Neodymium isotopic ratios were measured in oxide form, fractionation corrected to $^{146}NdO/^{144}NdO = 0.72225$ ($^{146}Nd/^{144}Nd = 0.7219$) and are reported relative to $^{143}Nd/^{144}Nd = 0.511856 \pm 0.000016$ ($n = 19$) for the La Jolla Nd Standard. Lead isotopic ratios were analyzed using the double-spike method to correct for mass fractionation during analyses; separate measurements of spiked and unspiked samples were made on different aliquots from the same dissolution. During the analysis period, the method produced the following results for NBS981: $^{206}Pb/^{204}Pb = 16.930 \pm 0.002$, $^{207}Pb/^{204}Pb = 15.490 \pm 0.003$ and $^{208}Pb/^{204}Pb = 36.700 \pm 0.009$ ($n = 11$). Analysis of BHVO-2 yielded 0.703485 ± 0.000004 for $^{87}Sr/^{86}Sr$, 18.653 ± 0.002 for $^{206}Pb/^{204}Pb$; 15.510 ± 0.002 for $^{207}Pb/^{204}Pb$; and $38.160 \pm <0.001$ for $^{208}Pb/^{204}Pb$.Total procedural blanks for Sr and Pb were 35 ng and 60 ng, respectively.

A set of 27 powders was investigated for *Re*—Os isotope systematics at State Key Laboratory of Isotope Geochemistry (SKLIG) at Guangzhou Institute of Geochemistry. These measurements used a Carius tube digestion method according to that of Li et al. (2010). Approximately 0.5–2 g of powdered sample was spiked with ^{185}Re and ^{190}Os and digested in reverse Aqua Regia in sealed Carius tubes at 240 °C for twenty-four hours. Osmium was separated using a single solvent extraction into CCl_4 prior to a back extraction into concentrated HBr. Finally, samples were microdistilled. Rhenium was then separated from the residual Aqua Regia using anion column chromatography.

In a later part of the study, a subset of 19 rock powders, free from any metal preparation, were crushed and powdered in alumina prior to HSE abundance and $^{187}Os/^{188}Os$ determination, at the SIGL. Samples with MgO contents >6 wt% were selected for Os-isotope and highly siderophile element (HSE) abundance analyses ($n = 19$). Approximately 800 mg of homogenized powder was combined with multi-element spikes (^{185}Re, ^{106}Pd, ^{194}Pt, ^{191}Ir, ^{99}Ru, ^{190}Os) prior to digestion in sealed borosilicate Carius tubes. The exceptions are $A210B_1 = 204$ mg, AW82214 = 381 mg, $A233D_1 = 353$ mg, and $A232B_1 = 712$ mg, which used the entirety of the remaining sample. Digestion within the Carius tubes used a 1:2 mixture of multiply Teflon distilled HCl and Os-purged HNO_3 heated to a maximum temperature of 270 °C for 72 h. Osmium was separated using a triple-extraction of CCl_4 and back-extracted into HBr (Cohen and Waters, 1996) prior to double microdistillation (Birck et al., 1997). The other HSE were recovered and extracted using column anion exchange separation techniques (Day et al., 2016).

Isotopic compositions of Os were measured on a ThermoScientific Triton thermal ionization mass spectrometer in negative ion mode. Rhenium, Pd, Pt, Ru and Ir were measured using an Cetac Aridus II desolvating nebuliser coupled to a ThermoScientific iCAP q ICP-MS. Offline corrections involved an oxide correction, an iterative

fractionation correction using $^{192}Os/^{188}Os = 3.08271$, a ^{190}Os spike subtraction, and a blank subtraction. Precision for $^{187}Os/^{188}Os$, determined by repeated measurement of the UMCP Johnson-Matthey standard during the course of the campaign was better than ±0.3% (2 St. Dev.; 0.11371 ± 29; $n = 5$). Measured Re, Ir, Pt, Pd and Ru isotopic ratios for sample solutions were corrected for mass fractionation using the deviation of the standard average run on the day over the natural ratio for the element. External reproducibility on HSE analyses using the iCAP q was better than 1% for 0.5 ppb solutions and all reported values are blank corrected. The total procedural blank run with the samples had $^{187}Os/^{188}Os$ of 0.157 ± 0.005, with quantities (in picograms) of 20 [Re], 17 [Pd], 17 [Pt], 17 [Ru], 0.6 [Ir] and 0.23 [Os]. These blanks resulted in corrections of <5% for Pd, Ir and Os, up to 20% corrections for Re and as much as 30% blank corrections for Ru and Pt. Data quality was monitored with measurement of BHVO-2 ($^{187}Os/^{188}Os = 0.15467 \pm 0.00015$), which show agreement with published $^{187}Os/^{188}Os$ values (Li et al., 2010, Li et al., 2014). The measurements of HSE (Table 1; Re = 0.650 ng/g, Pd = 3.19 ng/g, Pt = 8.01 ng/g, Ru = 0.125 ng/g, Ir = 0.124 ng/g, Os = 0.124 ng/g) are consistent with values from Meisel and Mosser (2004) and Day et al. (2021).

Twelve samples were analyzed at both the SIGL and SKLIG and, in general, there is excellent agreement for the Re ($R^2 = 0.993$), Os ($R^2 = 0.936$), $^{187}Re/^{188}Os$ ($R^2 = 0.931$), and $^{187}Os/^{188}Os$ ($R^2 = 0.986$) measurements and calculated γOs_t values ($R^2 = 0.969$) between the two labs (Fig. S1). Hence, although tungsten carbide was used in the processing of powders used at the SKLIG, there is no evidence for any W interference in the SKLIG data and so both datasets are considered without prejudice.

4. Results

4.1. Bulk-rock major element variations

Major element analyses are presented in Supplementary Table S1. The majority of lavas are basanite, and the remainder consists of alkali basalt, tephrite, hawaiite, mugearite, trachyandesite, trachyte, and rhyolite (Fig. 2; see also Fig. 3 in Panter et al., 2018). In detail, the bulk of continent-ocean transition Possession Islands and oceanic ABS lavas are highly alkaline, similar to basanites from the seamounts and Franklin and Beaufort islands in the Terror Rift region within the southern Ross Sea (Aviado et al., 2015). Moreover, both basanite suites mainly plot in the field for the Erebus Volcanic Province (Kyle et al., 1992; Martin et al., 2021). Samples in this study that were erupted on continental crust plot within the field for the MHp and most are basalts (Rocchi and Smellie, 2021). However, there are four evolved samples (Fig. 2), two are from a single isolated seamount in the eastern portion of the Adare Basin: sample D17–1 classifies as a weakly Si-undersaturated (0.1 wt% normative *nepheline*) trachyte (62 wt% SiO_2, $Na_2O + K_2O$ = 11.8 wt%) and sample D17–5 is a Si-oversaturated (25 wt% normative *quartz*) rhyolite (72 wt% SiO_2). The other two samples are a Si-oversaturated (6.5 wt% normative *quartz*) trachyte (67 wt% SiO_2) from the Adare Peninsula Volcanic Field (PRR-3831) and a Si-saturated (4 wt% normative *hypersthene*) trachyandesite (58 wt% SiO_2) from the Possession Islands (PRR-5166; Table S1).

The lavas define generally overlapping negative SiO_2, K_2O and Na_2O, and positive TiO_2, FeO* and CaO trends with increasing MgO, from c. 0.1 to 13.3 wt% (Fig. 3). These trends are similar to the basaltic to trachyte-rhyolite fractional crystallization trends of some, though not all, samples from the WARS volcanic provinces (e.g., Kyle et al., 1990; Armienti and Perinelli, 2010; Panter et al., 2021). Some of the basaltic samples (< 52 wt% SiO_2) from each lava suite are relatively unfractionated (> 8 wt% MgO) and could be representative of parental liquids to more differentiated lavas. A subtle difference among the continent-oceanic lava suites is discernable in the fractionation trends of the incompatible elements K and Na that are consistent with the relative alkalinity of the suites (Fig. 2). At >5 wt% MgO, ABS samples have the highest K_2O whereas Adare Peninsula samples have the lowest, and Possession Islands and HMp samples have intermediate K_2O contents (Fig. 3f). Similarly, the ABS and Possession Islands Na_2O values on average are higher than those of Adare Peninsula and HMp lavas (Fig. 3). Such differences, however, are not displayed by the fractionation trends of TiO_2 and CaO (see also Table S1).

4.2. Bulk-rock trace element abundances

All samples are enriched in incompatible trace elements relative to primitive mantle, similar to OIB (Fig. 4). Their overlapping concentration patterns partially overlap with, although are in lower absolute concentration than, southern Ross Sea and northern Victoria Land data (Aviado et al., 2015). On average, oceanic ABS and transitional Possession Islands lavas have higher absolute incompatible trace element abundances than continental lavas, consistent with the subtle differences in their alkali contents (Figs. 2 and 3). Moreover, ABS lavas on average have lower Th/La than the other lava suites. There are no clear differences in Nb/U and Ce/Pb among the lava suites; these ratios in lavas with >5 wt% MgO (32–93 and 21–94, respectively; Table S1) are around or above the canonical mantle values for OIB (Nb/U = 45 ± 10, Ce/Pb = 25 ± 5; Hofmann et al., 1986).

4.3. Strontium, Nd and Pb isotopes

The samples have relatively wide ranges of $^{87}Sr/^{86}Sr$ (0.70287–0.70331), $^{143}Nd/^{144}Nd$ (0.51280–0.51300) and $^{206}Pb/^{204}Pb$ (19.237–20.237) (Table S1; Fig. 5). These ratios are within the range of isotopic analyses for WARS lavas including those reported in previous continent-oceanic transect investigations (Panter and Castillo, 2007; Aviado et al., 2015; Panter et al., 2018). On average, the oceanic ABS and transitional Possession Islands lavas have slightly higher $^{143}Nd/^{144}Nd$ and lower $^{87}Sr/^{86}Sr$ than the continental Adare Peninsula lavas; this parallels the more alkaline character of the oceanic lavas described earlier (Fig. 2). However, their $^{206}Pb/^{204}Pb$ overlap. The ABS together with many Possession Islands samples also form linear arrays on plots of $^{207}Pb/^{204}Pb$ and $^{208}Pb/^{204}Pb$ versus $^{206}Pb/^{204}Pb$ (Fig. 5b and c) that are slightly lower than the Adare Peninsula lava suite. The two HMp lavas are split between the two groups, with the basalt from the Daniell Peninsula volcanic field of the Hallett Province (PRR-3839) being similar to Adare Peninsula lavas, whereas the basalt from the Melbourne Province further inland on the Malta Plateau (MA-117) being similar to ABS lavas.

As a whole, the samples show coherent negative $^{87}Sr/^{86}Sr$ versus $^{143}Nd/^{144}Nd$ array and positive $^{207}Pb/^{204}Pb$ and $^{208}Pb/^{204}Pb$ versus $^{206}Pb/^{204}Pb$ arrays that are typical of many oceanic lavas. They plot in the "focus zone" (FOZO; see also, Aviado et al., 2015; Panter et al., 2018), which is similar to "C" in Hanan and Graham (1996), where oceanic lavas converge in all permutations of the Sr-Nd-Pb isotope diagrams (Hart et al., 1992; Hauri et al., 1994). The FOZO component is considered to be a ubiquitous and most voluminous component in the OIB source (Hart et al., 1992; Hauri et al., 1994; Hanan and Graham, 1996; Stracke et al., 2005; Jackson et al., 2007; Castillo, 2015). Importantly, the FOZO component has been considered as young HIMU and exhibits many compositional features of HIMU (Thirlwall, 1997; Stracke et al., 2005; Castillo, 2015). In contrast, a number of previous studies have interpreted such WARS isotopic signature instead as HIMU-type (Panter et al., 2006; Nardini et al., 2009; Martin et al., 2013; Kipf et al., 2014; Aviado et al., 2015; Panter et al., 2018). Moreover, the new analyses have generally higher $^{143}Nd/^{144}Nd$ and lower $^{87}Sr/^{86}Sr$, $^{206}Pb/^{204}Pb$, $^{207}Pb/^{204}Pb$, and $^{208}Pb/^{204}Pb$ than some CVL and EARS lavas that are also characterized as HIMU-type compositions (Fitton and Dunlop, 1985; Rooney et al., 2014; Ngwa et al., 2017; Wembenyui et al., 2020).

Table 1
HSE abundances, ^{187}Re—^{187}Os, $^{187}Os/^{188}Os$, $^{87}Sr/^{86}Sr$, $^{143}Nd/^{144}Nd$, and $^{206}Pb/^{204}Pb$ for the northwest Ross Sea lavas.

Sample ID	Lab*	Location**	Regime	Long [° E]	Age*** (Ma)	MgO (wt %)	Re (ppb)	Pd (ppb)	Pt (ppb)	Ru (ppb)	Ir (ppb)	Os (ppb)	$^{187}Re/^{188}Os$	2SE	$^{187}Os/^{188}Os_m$	2SE	γ Os_t	$^{187}Os/^{188}Os_t$	$^{87}Sr/^{86}Sr$	$^{143}Nd/^{144}Nd$	$^{206}Pb/^{204}Pb$	Fo#	$\partial^{18}O$ ol# SIMS
BHVO-2	SIGL					7.4	0.650	3.191	8.008	0.125	0.124	0.124	25.3	0.4	0.15467	0.00015	21		0.703485		18.653		
D2–1	SIGL	ABS	Oceanic	171.8	15.93	9.6	0.181	0.895	0.569	0.071	0.022	0.017	53	1	0.29368	0.00079	119	0.2798	0.703282	0.512968		*87*	*5.25*
D2–1	SKLIG	ABS	Oceanic	171.8	15.93	9.6	0.142					0.015	48	1	0.25730	0.00070	92	0.2450					
D3–1	SKLIG	ABS	Oceanic	172.0	4.61	4.7	0.106					0.002	253	4	0.79790	0.00410	509	0.7766					
D4–1	SIGL	ABS	Oceanic	172.3	3.35	13.3	0.250	0.876	0.730	0.787	0.250	0.387	3.12	0.05	0.12900	0.00009	1.00	0.1288	*0.702869*	*0.512998*	*19.237*	*90*	*5.04*
Rpt	SIGL	ABS	Oceanic	172.3	3.35	13.3	0.268	0.842	0.730	1.212	0.442	0.762	1.69	0.03	0.12548	0.00025	−1.7	0.1254					
D4–1	SKLIG	ABS	Oceanic	172.3	3.35	13.3	0.199					0.233	4.1	0.1	0.12960	0.00040	1.4	0.1294					
D4–3	SIGL	ABS	Oceanic	172.3	2.51	9.9	0.187	0.902	0.160	0.038	0.088	0.035	25.6	0.4	0.17001	0.00019	32	0.1689	0.703124	0.512878	19.449	*79*	*5.43*
D6–1	SKLIG	ABS	Oceanic	171.9	*0.3*	5.9	0.408					0.004	462	7	0.37420		191	0.3717	0.702895	0.512950	20.207		
D7–1	SKLIG	ABS	Oceanic	171.9	0.32	3.2	0.251					0.001	1305	20	0.34050		162	0.3339	0.702859	0.512952	20.237		
D9–1	SKLIG	ABS	Oceanic	171.9	2.86		0.284					0.008	161	2								*79*	*5.05*
D12–1	SIGL	ABS	Oceanic	172.6	2.89	11.0	0.336	0.673	0.229	0.102	0.047	0.061	26.9	0.4	0.18300	0.0012	43	0.1817	*0.702774*	*0.513001*	*20.111*	*84*	*5.35*
D12–1	SKLIG	ABS	Oceanic	172.6	2.89	10.7	0.282					0.008	165	2	0.19460	0.0007	46	0.1863					
D15–1	SKLIG	ABS	Oceanic	172.7	3.12	7.0	0.329					0.008	200	3	0.20810	0.0016	55	0.1977	0.702953	0.512952	19.863		
D16–1	SKLIG	ABS	Oceanic	172.8	2.76	6.7	0.366					0.006	305	5	0.25940		93	0.2456	0.702890	0.512961	20.169		
PRR 3839	SIGL	PI	Transitional	169.6	*6*	9.4	0.234	0.900	0.351	0.025	0.024	0.016	73	1	0.19900	0.00140	50	0.1919	0.703083	0.512914	20.038	*84*	*4.89*
PRR-3839	SKLIG	PI	Transitional	169.6	*6*	9.1	0.195					0.009	107	2	0.19660	0.00110	46	0.1861					
PRR 3842	SIGL	PI	Transitional	171.1	*<0.4*	9.3	0.415	1.215	0.218	0.048	0.038	0.063	31.9	0.5	0.14395	0.00026	12.7	0.1437	0.702946	0.512944	20.18	*81*	*5.06*
PRR 5169	SIGL	PI	Transitional	171.1	*0.3*	9.5	0.247	0.581	0.223	0.060	0.037	0.068	17.6	0.3	0.14041	0.00025	10.0	0.1403	0.702938	0.512933	20.115	*83*	*4.82*
PRR 5171	SIGL	PI	Transitional	171.1	0.33	9.5	0.307	0.691	0.244	0.045	0.030								0.702944	0.512940		*82*	*4.71*
PRR 3872	SIGL	PI	Transtional	171.2	*0.16*	3.1	0.185	1.071	0.262	0.085	0.053	0.024	37	1	0.18444	0.00068	44.5	0.1843	0.703044	0.512954	19.743	*75*	*5.23*
A232B	SIGL	AP	Continental	170.3	*10.2*	7.1	0.191	0.782	0.157	0.009	0.011	0.005	183	3	0.55500	0.00290	309	0.5220	*0.703724*	*0.512874*	*19.432*	*81*	*5.30*
A232B	SKLIG	AP	Continental	170.3	*10.2*	7.1	0.139					0.005	134	2	0.38310	0.00200	182	0.3596					
A210B	SIGL	AP	Continental	170.2	*10.2*	13.1	1.381	1.582	0.668	0.433	0.265	0.206	32.4	0.5	0.14654	0.00024	10.6	0.1410	*0.703440*	*0.512891*	*19.363*		
A210B	SKLIG	AP	Continental	170.2	*10.2*		1.130					0.183	29.9	0.4	0.14330	0.00290	8.4	0.1382					
A223D	SIGL	AP	Continental	170.7	*12.2*	7.5	0.403	1.271	0.298	0.033	0.039	0.019	101	2	0.15060	0.00140	1.8	0.1298					
A233D	SKLIG	AP	Continental	170.7	2.21	7.5	0.297					0.020	70	1	0.15010		15.6	0.1475					
P74833	SIGL	AP	Continental	170.1	10.6	8.0	0.344	1.152	0.057	0.006	0.012	0.003	668	10	1.1660	0.0180	728	1.0552	0.703803	0.512814	19.211	*70*	*5.15*
P74833	SKLIG	AP	Continental	170.1	10.6	8.0	0.226					0.002	683	10	0.64700	0.00400	327	0.5443					
P74794	SIGL	AP	Continental	170.1	10.2	9.4	0.387	0.823	0.181	0.046	0.033	0.045	42	1	0.16857	0.00060	26.7	0.1615	0.703612	0.512859	19.459	*80*	*5.33*
P74794	SKLIG	AP	Continental	170.1	10.2	9.4	0.251					0.014	88	1	0.17960		29.3	0.1648					
24,583	SKLIG	HMp	Continental	163.4	0.18	9.6	0.187					0.013	71	1	0.13131	0.00043	2.8	0.1311					
24,591	SKLIG	HMp	Continental	163.4	*2.3*		0.307					0.057	26.0	0.4	0.12775	0.00025	−0.6	0.1268					
PRR-5194	SKLIG	HMp	Continental	170.3	*6.4*		0.087					0.004	113	2	0.21800		62	0.2067					
A225C-2	SKLIG	HMp	Continental	171.1	0.24		0.354					0.013	131	2	0.20580		61	0.2053					
AW82214	SIGL	HMp	Continental	171.2	*<1.5*	9.8	0.205	0.843	0.850	0.050	0.058	0.021	48	1	0.15861	0.00055	23.4	0.1574	*0.702884*	*0.512945*	*19.851*		
AW82214	SKLIG	HMp	Continental	171.2	*<1.5*	9.8	0.132					0.025	25.3	0.4	0.14590	0.00040	13.9	0.1453					
A277	SKLIG	HMp	Continental	169.6	*9.5*		0.147					0.001	634.1	9.5	0.61890	0.00890	292	0.4996					
82,107	SKLIG	HMp	Continental	168.3	*10.88*		0.136					0.009	80	1	0.48230	0.00120	267	0.4685					
A214B	SKLIG	HMp	Continental	170.0	*7.5*		0.160					0.002	480	7	0.26920	0.00130	73	0.2201				*76*	*5.10*
A216	SKLIG	HMp	Continental	169.8	*7.5*		0.246					0.003	472	7	0.21630		30.5	0.1663					
25,679	SKLIG	MP	Continental	165.5	*0.826*		0.261					0.017	74	1	0.21650		69	0.2155					
MA-117	SIGL	MP	Continental	167.6	15	8.5	0.395	0.778	0.214	0.028	0.021								*0.703751*				
MA-117	SKLIG	MP	Continental	167.6	15		0.299					0.012	126	2	0.43570	0.00190	217	0.4045	0.703282	*0.512824*	*19.320*	*79*	*5.39*
81,510	SIGL	MP	Continental	164.6	*7*	8.4	0.193	0.577	0.238	0.024	0.064	0.013	72	1	0.16500	0.00150	22.8	0.1566					
81,510	SKLIG	MP	Continental	164.6	*7*	8.4	0.136					0.009	76	1	0.14800	0.00120	9.4	0.1395					

Notes: *SIGL = Scripps Isotope Geochemistry Laboratory; SKLIG = State Key Laboratory of Isotope Geochemistry; **AB = Adare Basin; PI = Possession Islands; AP = Adare Peninsula; HP = Hallett Peninsula; MP = Malta Plateau; ***Samples with ages (Ma) shown in italics are approximated based on field relationships and proximity to dated samples within the same volcanic field. Dated samples and the approximated ages were derived from the following sources: Armstrong (1978); Muller et al. (1991); Esser and Kyle (2002); Armienti et al. (2003); Mortimer et al. (2007); Smellie et al. (2011); Panter et al. (2018); Smellie and Rocchi (2021); Merle et al. (2022). #Forsterite content (Fo), $\delta^{18}O$ of olivine and Sr-Nd-Pb isotope data in italics are from Panter et al. (2018); see supplementary Table S1 for details of the analyses.

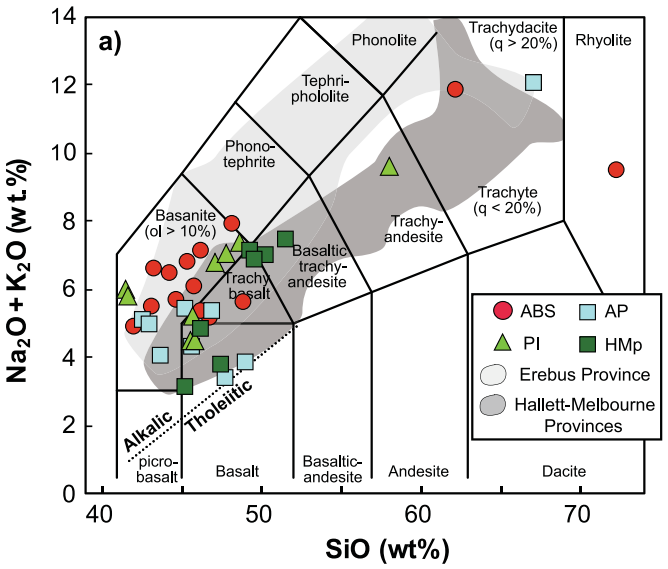

Fig. 2. Total alkalis versus silica (after Le Bas et al., 1986) for the northwest Ross Sea lavas. Alkalic-tholeiitic line as in Macdonald and Katsura (1964). Light grey region represents data from Erebus Province (LeMasurier and Rex, 1991; Kyle et al., 1992); dark grey shaded region shows data from Hallett and Melbourne provinces (LeMasurier and Thompson, 1990; Armienti et al., 1991). Other symbols used: ABS = Adare Basin seamounts; PI = Possession Islands; AP = Adare peninsula; HMp = Hallett-Melbourne provinces.

4.4. Rhenium-Os isotopes and HSE abundances

The HSE abundance patterns for the WARS basaltic lavas (MgO = 5.9 to 13.3 wt%) are similar to those of basaltic melts that have experienced differing extents of fractional crystallization (Day, 2013). The most compatible HSE (Os, Ir, Ru) show decreasing abundance from the highest in ABS and Adare Peninsula lavas at ~0.1 × Primitive Mantle (PM) to the lowest in Adare Peninsula lavas also at 0.001 × PM (Table 1; Fig. 6). This trend is also evident for Pt. The lowest Os, Ir and Ru concentrations are observed in the AP samples (P74833 and A232B), which also have some of the lowest MgO contents. Compared to Os, Ir, Ru, and Pt, Pd and Re abundances are higher and show significantly less variability at ~0.1 to 1 × PM values (Table 1). The HSE abundance patterns of WARS basaltic lavas are different from those of basanites from Hut Point Peninsula of Ross Island (Fig. 1a), which show a concave up pattern with generally higher Os but lower total Re abundances (Day et al., 2019).

The samples show a large range in measured $^{187}Os/^{188}Os_m$ (0.1255 to 1.166) and $^{187}Re/^{188}Os$ (1.7 to 1305; Table 1) and show significant scatter on a $^{187}Re/^{188}Os$-$^{187}Os/^{188}Os_m$ diagram (Fig. 7). Samples with low Os content (<0.10 ppt) have generally more radiogenic $^{187}Os/^{188}Os_m$, consistent with previous studies of OIB lavas (Day, 2013). However, the highest and lowest $^{187}Os/^{188}Os_m$ values are not from low Os samples and both SIGL and SKGIL laboratories generated consistent duplicate analyses of such samples. Moreover, the $^{187}Os/^{188}Os_m$ data show some systematic patterns. Adare Peninsula samples have the widest range in $^{187}Os/^{188}Os_m$ (0.1433 to 1.166) followed by ABS samples (0.1290 to 0.7979). Possession Island and HMp samples fall within this range. Adare Peninsula sample A210B and ABS sample D4–1 with the highest MgO (both at c. 13 wt%) have low $^{187}Os/^{188}Os_m$ of 0.1465 and 0.1255, respectively, that overlap with the $^{187}Os/^{188}Os_m$ of ultramafic xenoliths (0.1279–0.1374), slightly lower than those of basanites (0.1432–0.1595), from the Hut Point Peninsula (Day et al., 2019). Adare Peninsula sample RRR 3872 and ABS samples D7–1 and D3–1 with the lowest MgO (<5 wt%) have a large range of $^{187}Os/^{188}Os_m$ (0.1844, 0.3405 and 0.7979, respectively). In general, $^{187}Os/^{188}Os$ does not correlate well with MgO content, but samples with radiogenic values tend to have low Os and MgO contents. Moreover, age-corrected $^{187}Os/^{188}Os_t$ has a positive, but highly curved relationship with $^{87}Sr/^{86}Sr$, but a negative, but highly curved relationship with both $^{143}Nd/^{144}Nd$ and $^{206}Pb/^{204}Pb$ (Fig. 8).

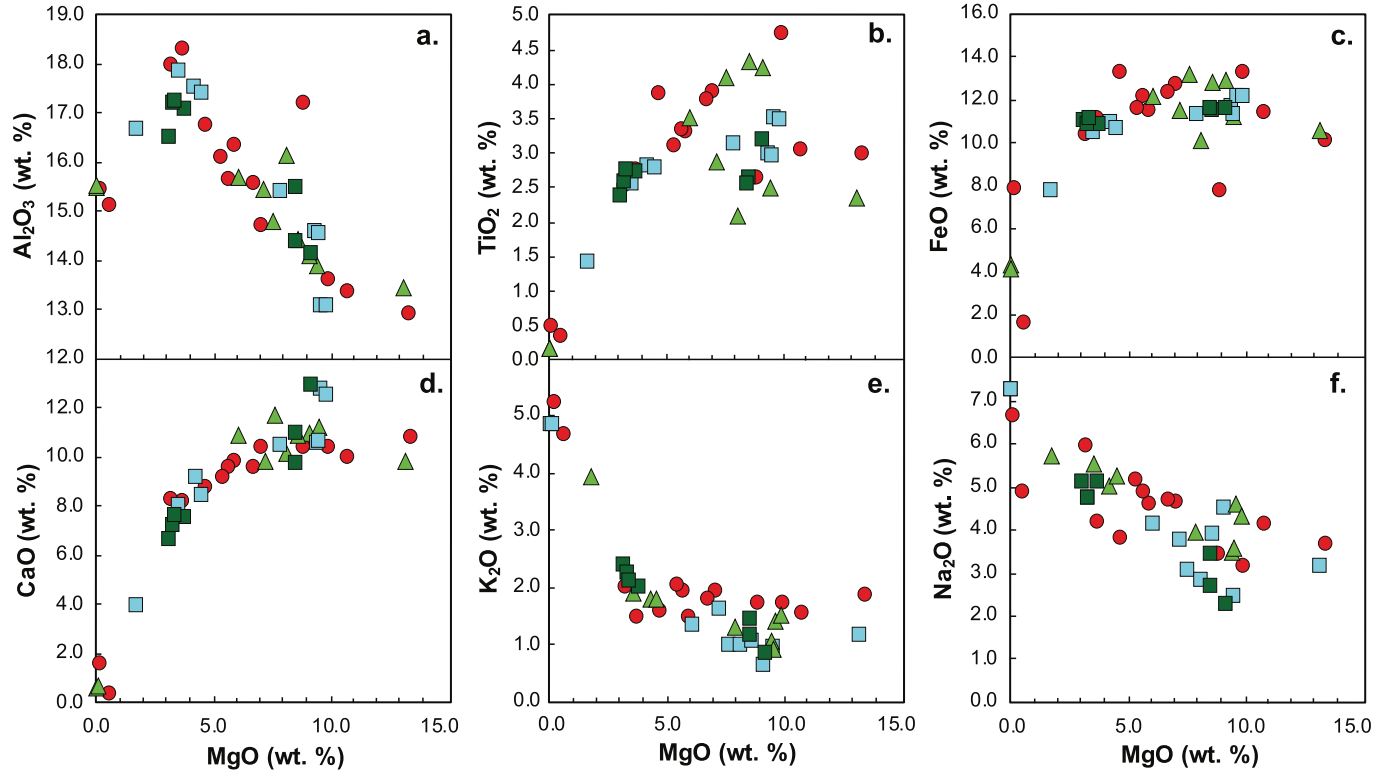

Fig. 3. MgO versus other oxides for lavas from the northwest Ross Sea region. Data from this study and Panter et al. (2018).

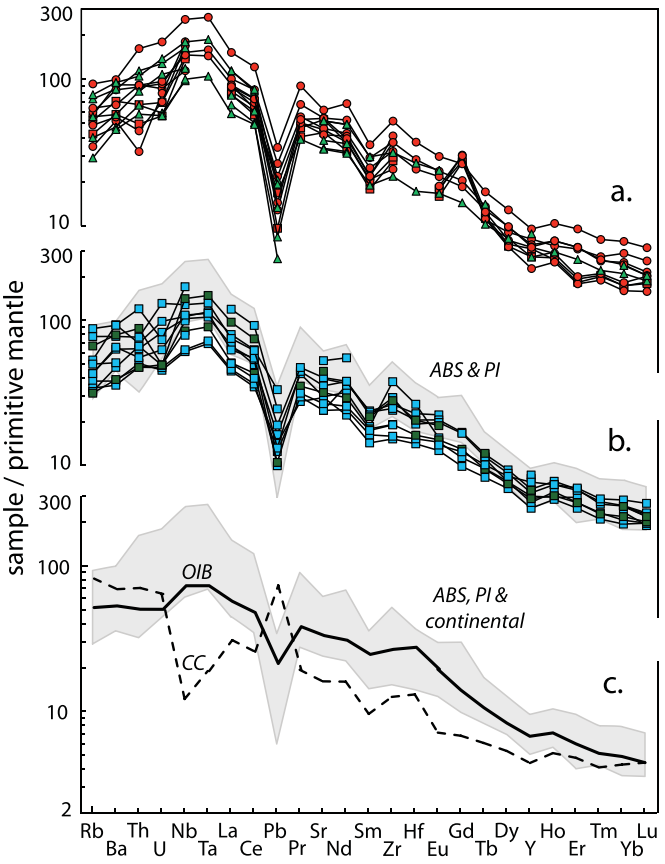

Fig. 4. Primitive mantle (McDonough and Sun, 1995) –normalized incompatible trace element concentration patterns for a) ABS and PI lavas, b) AP and HMp lavas and c) OIB (Sun and McDonough, 1989) and continental crust (CC; Rudnick and Gao, 2014). Data from Table S1. The shaded are in b) represents the total range of ABS and PI lavas and in c) represents all the lava samples. Symbols as in Figs. 1 to 3.

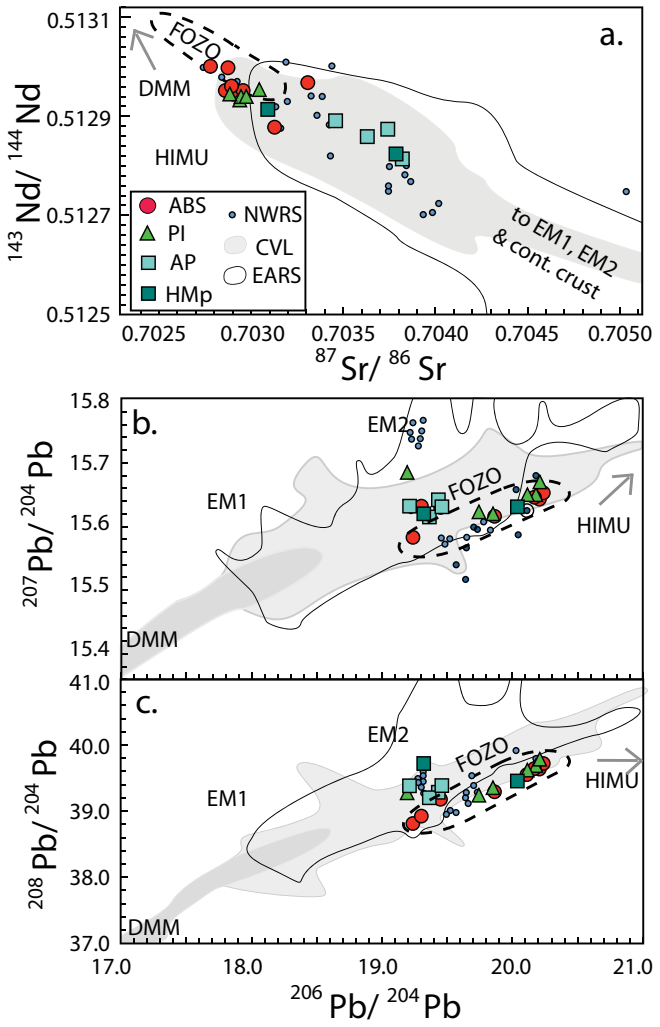

Fig. 5. a. $^{143}Nd/^{144}Nd$ versus $^{87}Sr/^{86}Sr$ diagram, b. $^{208}Pb/^{204}Pb$ versus $^{206}Pb/^{204}Pb$ diagram and c. $^{207}Pb/^{204}Pb$ versus $^{206}Pb/^{204}Pb$ diagrams for the northwest Ross Sea (NWRS) lavas. Shown for reference are mantle source components DMM (Workman and Hart, 2005), EM1 and EM2 (Salters and Sachi-Kocher, 2010), HIMU (Stracke et al., 2003) and FOZO (Hauri et al., 1994; Stracke et al., 2005) and fields for the East African Rift System (EARS; Castillo et al., 2020; Rooney, 2020 and references therein) and the Cameroon Volcanic Line (CVL; darker shades of grey in b. and c. represent the most continental crust contaminated Bamoun Plateau lavas; Asaah et al., 2015; Atouba et al., 2016; Wembenyui et al., 2020 and references therein) lavas. Sources of other data and symbols as in Figs. 1 to 3.

5. Discussion

Panter et al. (2018; see also Panter and Castillo, 2007) showed systematic compositional variations of WARS lavas from the same continent-oceanic transect. Their model to explain these variations, based primarily on whole-rock geochemical and Sr-Nd-Pb isotopes as well as O isotopes of olivine, rules out shallow-level crustal contamination. Instead, they invoked melting of metasomes followed by melt-peridotite reaction that decreases oceanward within the progressively thinned lithosphere that was developed in several extensional phases over a period of c. 90 Ma. The new results compliment and extend their existing data and also show new systematic compositional variations from the continent to ocean transition.

5.1. Fractional crystallization and crustal contamination

To constrain the origin of the compositional variations of the transect lavas, it is first necessary to consider whether magmatic differentiation and/or crustal contamination processes have modified parental melt compositions. The systematic behavior of major oxides and trace elements with decreasing MgO contents of lavas (Figs. 3 and 6) indicate fractional crystallization is most likely responsible for some of the geochemical and lithological variations observed in WARS lavas (see also, e.g., Nardini et al., 2009; Martin et al., 2013; Aviado et al., 2015; Panter et al., 2018). As the HSE are compatible elements, their concentrations in the continental-oceanic transect lavas are affected by fractional crystallization. For instance, the decrease in HSE concentrations from the most primitive (i.e., MgO >10%) to the most evolved (i.e., MgO <5 wt%) lavas, such as the sharp decrease in Os content with decreasing MgO (Fig. 7b), can be modeled through increasing degrees of fractional crystallization of likely silicate, oxide and sulfide phases (Fig. 6).

Melts undergoing fractional crystallization, however, can also be further modified by crustal assimilation as they rise towards the surface, especially from hydrous or silica-rich continental crust. Although HSE abundances are usually controlled by fractional crystallization, crustal assimilation has a generally dilutional effect on HSE abundances that will disproportionately increase radiogenic $^{187}Os/^{188}Os$ (e.g., Fig. 7; Day, 2013). Continental crust $^{187}Os/^{188}Os$ is typically in the range of 1.1 ± 0.2 (Peucker-Ehrenbrink et al., 2003), much higher than primary melts of the primitive mantle $^{187}Os/^{188}Os$ of 0.1296 (Meisel et al., 2001). Hence, assimilation of continental crust by a fractionating primitive melt with a low concentration of radiogenic Os will severely increase its $^{187}Os/^{188}Os$. This makes the *Re*—Os isotope system a highly

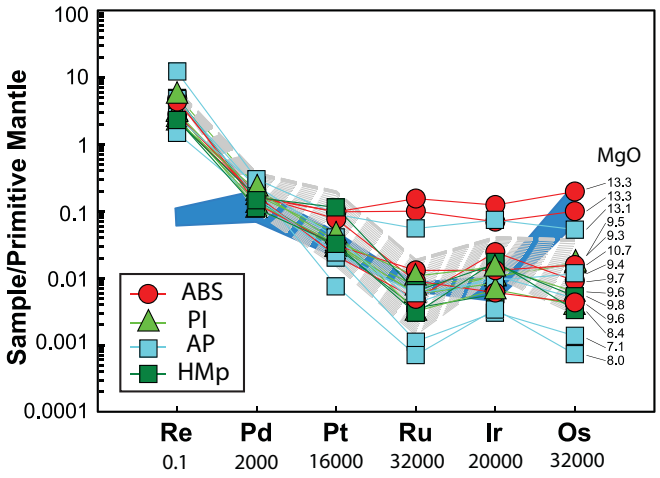

Fig. 6. Primitive mantle-normalized HSE abundance patterns of the northwest Ross Sea lavas. Shown in the shaded grey field is a crystallization model assuming sulfide precipitation, using D-values noted beneath the individual elements; also shown in blue field is the abundance pattern of all basanites from the Hut Point Peninsula of Ross Island (Fig. 1a; Day et al., 2019). Primitive mantle normalization from Day et al. (2017). Small numbers on the right side of the diagram are MgO contents of the samples analyzed for HSE. (For interpretation of the references to colour in this figure legend, the reader is referred to the web version of this article.)

sensitive indicator of crustal contamination in evolving basaltic magmatic systems.

Oxygen isotopes are also sensitive tracers of crustal contamination and the type of crustal lithology, as O is a major component of silicate rocks (c. >46 wt%). Various igneous reservoirs reveal that increasing SiO_2 content of rock correlates with increasing $^{18}O/^{16}O$ typically expressed relative to a standard (or as $\delta^{18}O$), but that hydrothermal alteration by meteoric water at higher latitudes can lead to a significant depletion in $\delta^{18}O$ values of rocks and minerals (Craig, 1961; Muehlenbachs et al., 1974), especially of hydrothermally altered lavas. Antarctic precipitation has been well-established to have strongly negative $\delta^{18}O$ (as low as −35‰; Gonfiantini and Picciotto, 1959; Stewart, 1975; Kellogg et al., 1991; Antibus et al., 2014), but typical lithologies in continental crust, such as those found within the Transantarctic Mountains have highly positive $\delta^{18}O$ values (c. +10‰; Molzahn et al., 1996). Such a wide range of $\delta^{18}O$ for potential assimilants, combined with $^{187}Os/^{188}Os$ data, can be used to assess the type of crustal contamination in the high-latitude WARS setting.

Continental Adare Peninsula lavas have some of the lowest HSE abundances (especially Os, Ir, Ru) and the largest range in $^{187}Os/^{188}Os_m$ relative to the remainder of our sample suite (Figs. 6 and 7). The olivine grains in Adare Peninsula samples also have relatively low Fo contents (Panter et al., 2018; Fig. 10a) and although the Adare Peninsula lavas have a large range of MgO contents, the sample with the highest MgO has more radiogenic age-corrected $^{187}Os/^{188}Os_t$ (i.e., A210B = 13.1 wt% MgO, $^{187}Os/^{188}Os = 0.1382$) than typical mantle values. Similarly, the high MgO (>9 wt%) HMp continental lavas have elevated $^{187}Os/^{188}Os_t$ (0.1311–0.1574), and their olivine grains have low Fo contents (Figs. 7 and 10a). By comparison, the most primitive ABS oceanic lava (D4–1, MgO = 13.3 wt%) has the highest Os abundance (on average ~ 0.46 ng/g), unradiogenic $^{187}Os/^{188}Os_t$ (0.1254–0.1294) and olivine grains with the highest Fo content (up to Fo_{90}) among the sample suite. These indicate that, although the continental lavas are mostly differentiated, to a first order they have more radiogenic $^{187}Os/^{188}Os$ than the oceanic samples.

The $^{187}Os/^{188}Os_t$ of all of the samples analyzed range from 0.1254 to 1.055, and this can be produced by mixing between a primary depleted mantle melt and continental crust with $^{187}Os/^{188}Os$ values of ~0.1245 and 3.5, respectively (Molzahn et al., 1996; Day et al., 2021. The $\delta^{18}O$ values of the samples, however, have a limited range of 5.2 to 5.4‰, well within the average 5.2 ± 0.25‰ for olivine grains from northwest Ross Sea basalts (Panter et al., 2018) and similar to expected mantle values for olivine (Mattey et al., 1994). Based on such Os and O isotope constraints, our model calculations identify a contaminant with a $\delta^{18}O$ value similar or close to that of primary mantle melt that is typically 5.3 ± 0.3‰ (King et al., 1998). Moreover, the alkaline lavas have distinctive positive Nb and Ta but negative Pb and Rb concentration anomalies that are the opposite of typical old, differentiated and geochemically enriched continental crust (Fig. 4). The Nb/U and Ce/Pb ratios of primitive lavas (MgO >5 wt%) additionally plot around or above canonical mantle values for OIB (Fig. 9c and d), unlike the continental crust that plots below such mantle values. The amount of contamination in the model is also up to c. 100%, and such a significant quantity of continental crust should have modified the elemental and Sr-Nd-Pb isotope compositions of contaminated samples. Since this is not observed, particularly in sample P78433 with the highest $^{187}Os/^{188}Os_t$ value of 1.055 (i.e., with MgO = 8 wt%; $^{87}Sr/^{86}Sr = 0.7038$; $^{143}Nd/^{144}Nd = 0.51281$), the contaminant must have been mafic and geochemically depleted relative to the bulk silicate Earth (BSE; $^{87}Sr/^{86}Sr$ c. 0.7045; $^{143}Nd/^{144}Nd = 0.51264$). The contaminant, therefore, is most likely to be a ~ mafic component representing a modified and relatively young (juvenile) Antarctic lithospheric component with high Re/Os (Fig. 10b). The trace element composition of this component is also most likely enriched in incompatible trace elements, similar to that of WARS alkaline lavas. Along similar lines, Day et al. (2019) have proposed that the CLM beneath West Antarctica was melt-modified prior to WARS formation based on the Os and He isotopic and elemental data and petrology of a suite of xenoliths and lavas from the Hut Point Peninsula, suggesting similar sources for radiogenic Os. That is, the CLM beneath WARS was partially replaced and is, thus, relatively younger than that beneath the Transantarctic Mountains and Marie Byrd Land.

It must also be noted that the transitional Possession Islands lavas and oceanic ABS sample D4–1 have lower $\delta^{18}O$ values (down to +4.7‰) and wide ranges of $^{187}Os/^{188}Os_t$ (0.1254–0.1919), suggesting that a few transect lavas may have additionally assimilated a limited quantity (≤ 20%) of hydrated oceanic crust (HOC curve) similar to the altered mugearite sample MB32.11 with a low $\delta^{18}O$ value of +1.8‰ (Panter et al., 2018).

5.2. *Additional evidence for a continental lithospheric mantle contribution*

Many of our continental-oceanic transect samples were previously analyzed by Panter et al. (2018), who rejected crustal assimilation as a mechanism to explain the geochemical trends of the samples in favor of melt and modified CLM reaction. Our new HSE and *Re*—Os isotope data, combined with previously published O isotope data, indicate that contamination by a melt-modified CLM indeed plays a role in the petrogenesis of the northwest Ross Sea lavas. The new data also highlight that the first order Sr-Nd-Pb isotope variations in WARS lavas are due to juvenile CLM contamination.

In general, $^{87}Sr/^{86}Sr$ increases while $^{143}Nd/^{144}Nd$ and $^{206}Pb/^{204}Pb$ decrease from an oceanic to a continental setting, suggesting two separate sources (Fig. 9). Lanthanum/Sm ratio decreases in the same direction, indicating that ABS lavas are derived from a more geochemically enriched source than HMp lavas, or are generated through a smaller degree of partial melting of the same source. Most of the samples also plot between the two model isochrons showing the decay of the ^{187}Re—^{187}Os system in potential contaminant reservoirs suggesting Proterozoic to Cretaceous aged contaminant crustal sources (Fig. 7). As the continental-oceanic samples do not form a single isochron that would be consistent with an intermediate crystallization age, we suggest that mixing between a primary melt and juvenile CLM to varying degrees is the likely cause of these variations.

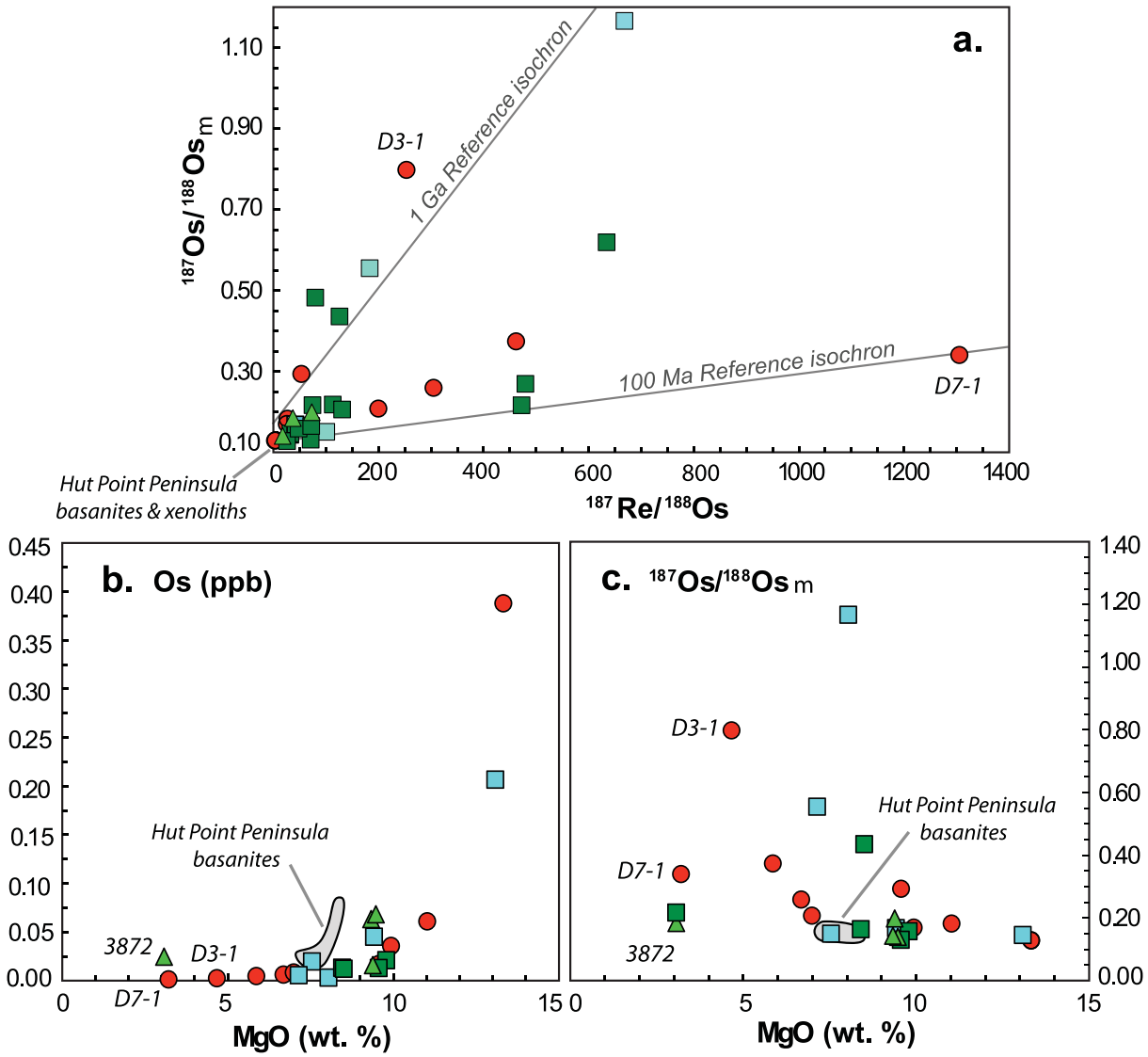

Fig. 7. a. Measured $^{187}Os/^{188}Os_m$ versus $^{187}Re/^{188}Os$, b. MgO versus Os and c. MgO versus $^{187}Os/^{188}Os_m$ diagrams for the northwest Ross Sea lavas. Shown in a. are modeled 100 Ma and 1 Ga reference isochron lines assuming a chondritic initial value. Also shown for reference are $^{187}Os/^{188}Os_m$ for basanites from the Hut Point Peninsula of Ross Island (Fig. 1a; Day et al., 2019). Mantle xenoliths ($^{187}Os/^{188}Os_m = 0.1279–0.1374$) brought up by the basanites are not shown in b. and c. as they have high MgO contents (23–47 wt%); basanites and mantle xenoliths plot at the bottom left corner in a. Symbols as in Figs. 1 to 3.

The highly curved relationships between age-corrected $^{187}Os/^{188}Os_t$ and Sr-Nd-Pb isotopes indicate crustal contamination or mixing between a primary melt and juvenile CLM (Fig. 8). The extreme curvature of the mixing arrays (Langmuir et al., 1978) restricts the Sr and Nd isotopic ratios of primary melt to be more geochemically depleted than BSE, and more so than the juvenile mantle contaminant. These inferences are consistent with the model inferred from Os and O isotopes that additionally requires the contaminant to be mafic (Fig. 10b). This component most likely originated from, for example, an asthenospheric mantle that had also been previously enriched (Hole, 1988; Finn et al., 2005; Košler et al., 2009; Panter et al., 2000, 2021), perhaps in the same manner that the transect lavas were generated; this will be discussed in more detail in the next section. It is noteworthy that this is the primary reason why Panter et al. (2018), despite the absence of the more definitive, continental crust-sensitive Os isotopes, proposed that the primary melt interacted with a modified CLM instead of typical continental crust.

Mixing calculations reveal that the curved $^{187}Os/^{188}Os_t$ versus Sr-Nd-Pb isotope arrays of the transect lavas can be modeled using a primary melt similar to that of FOZO (Hauri et al., 1994; Stracke et al., 2005) and juvenile CLM (FOZO-jCLM curve; Fig. 8) component represented by post-subduction alkaline lavas along the Antarctic Peninsula (Hole, 1988; Košler et al., 2009; Panter et al., 2023). Least contaminated are the primitive (≥10 wt% MgO), alkaline and incompatible trace element enriched ABS oceanic lavas such as ABS basalt D12–1 with high $^{143}Nd/^{144}Nd$ and $^{206}Pb/^{204}Pb$ but low $^{87}Sr/^{86}Sr$ (see also Panter et al., 2018). Note that the Sr-Nd-Pb isotope variations of some ABS lavas generally indicate direct mixing (ABS-jCLM curve) between ABS sample D12–1 and the same component (≤ 30% contamination) although both Sr and Pb isotopes of a couple of ABS samples are not consistent with such a mixing scenario. Note that the Sr—Pb isotope systematics are sensitive to seawater alteration (see also, Fig. 10b). An alternative possibility is that the primary melt coming from the mantle is inherently heterogeneous. Notably, the age-corrected $^{187}Os/^{188}Os_t$ of both basanites and mantle xenoliths from the juvenile CLM beneath the Hut Point Peninsula indeed have a much more restricted range (0.1279–0.1575; Day et al., 2019) than those of the transect lavas. Thus, Adare Peninsula continental lavas with the highest $^{87}Sr/^{86}Sr$ but the lowest $^{143}Nd/^{144}Nd$ among northwest Ross Sea lavas (Nardini et al., 2009; Martin et al., 2013; Aviado et al., 2015; Panter et al., 2018) that are the most contaminated in our model (> 90%) are alternatively proposed to trend

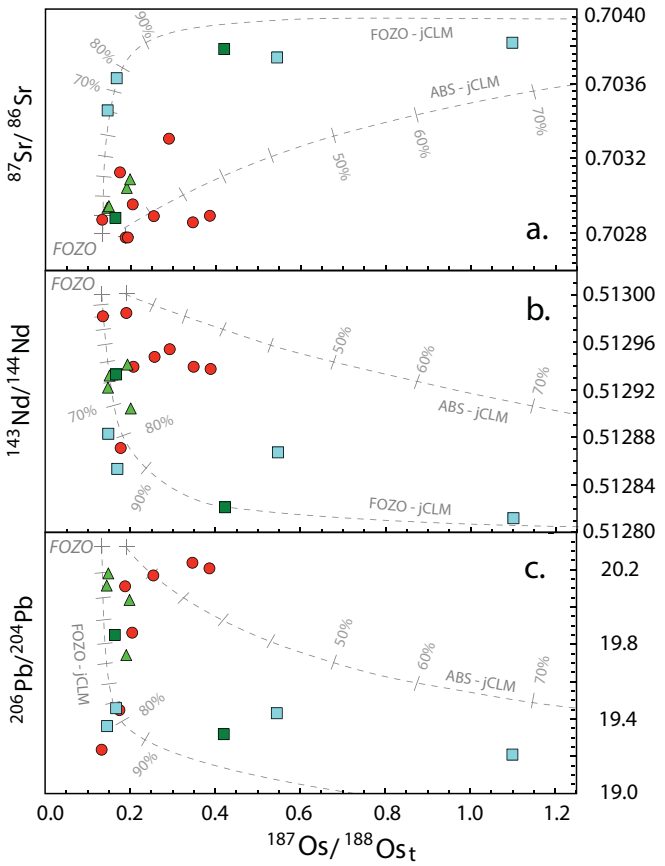

Fig. 8. Age-corrected $^{187}Os/^{188}Os_t$ versus a. $^{87}Sr/^{86}Sr$, b. $^{143}Nd/^{144}Nd$ and c. $^{206}Pb/^{204}Pb$ for the northwest Ross Sea lavas. Proposed models use a primary melt coming from a FOZO mantle component with Os = 3.1 ppb; Sr = 799 ppm; Nd = 55.1 ppm; Pb = 3.1 ppm; $^{187}Os/^{188}Os$ = 0.1276; $^{87}Sr/^{86}Sr$ = 0.7028; $^{143}Nd/^{144}Nd$ = 0.51295; $^{206}Pb/^{204}Pb$ = 20.4 (data after Molzahn et al., 1996; Stracke et al., 2003 and 2005) or ABS sample D12–1 with Os = 0.061 ppb; Sr = 1007 ppm; Nd = 48.4 ppm; Pb = 2.01 ppm; $^{187}Os/^{188}Os$ = 0.1830; $^{87}Sr/^{86}Sr$ = 0.70278; $^{143}Nd/^{144}Nd$ = 0.51300; $^{206}Pb/^{204}Pb$ = 20.11 (from Tables 1 and 2) and juvenile continental lithospheric mantle (jCLM) represented by post-subduction alkaline basaltic dike JR-16 with Os = 0.01 ppb; Sr = 672 ppm; Nd = 24.9 ppm; Pb = 3.86 ppm; $^{187}Os/^{188}Os$ = 3.5; $^{87}Sr/^{86}Sr$ = 0.70395; $^{143}Nd/^{144}Nd$ = 0.51282; $^{206}Pb/^{204}Pb$ = 18.857 (data after Molzahn et al., 1996; Kostel et al., 2009). Symbols as in Figs. 1 to 3. The bulk of data generally follow or plot between two model mixing curves FOZO – jCLM and ABS – jCLM. See text for discussion.

towards enriched mantle 1 and 2 components (EM1 and EM2, respectively; Fig. 5). Although our preferred model highlights the FOZO-like composition of alkaline lavas, a compositionally heterogeneous partial melt from the previously subducted slab sensu *lato* is permissible. This is because FOZO is the most voluminous, common component in such a melt and it can be produced through mixing or homogenization of the various mantle end-components with different "flavors" (e.g., Hart et al., 1992; Hauri et al., 1994; Stracke et al., 2005; Hofmann, 2014; Castillo, 2015). Such homogenization process most likely occurs when deep upwelling mantle melts encounter the thick and relatively cold continental lithosphere. The DMM component may also be involved but is not required as the main source of FOZO, the previously subducted oceanic lithospheric mantle, is simply a metamorphosed portion of DMM (Castillo, 2015). In any case, the ranges of $^{87}Sr/^{86}Sr$, $^{143}Nd/^{144}Nd$, $^{206}Pb/^{204}Pb$, and $^{187}Os/^{188}Os_t$ of the Possession Islands, HMp and differentiated ABS lavas fall between the two extremes.

5.3. The mantle source of WARS alkaline lavas

Kipf et al. (2014) proposed two distinct sources for the alkaline lavas from seamounts in the Amundsen Sea, off the West Antarctic margin (Fig. 1a). They proposed an ancient plume material that was initially accreted to the base of continental lithosphere for the HIMU isotopic signature of Marie Byrd Land seamount lavas and a recycled continental raft for the EM2 signature of Peter I Island lavas. As discussed previously, however, a continental crust source for our alkaline lavas is not supported by the trace element and combined Os and O isotopic data. Instead, models for the origin of WARS alkaline magmatism can be generally summarized into a question of whether the magmas come from either a mantle plume or a subduction fluid-metasomatized CLM source.

As noted earlier, the Sr-Nd-Pb isotope and incompatible trace element signatures of WARS lavas have been interpreted as indicative of a HIMU-type mantle plume source (Kyle et al., 1992; Rocholl et al., 1995; Sims et al., 2008; Kipf et al., 2014; Phillips et al., 2018). However, some studies have shown that both geochemical and geophysical indicators of an upwelling plume or fossilized plume are lacking in the Ross Sea region (Nardini et al., 2009; Aviado et al., 2015; Panter et al., 2018; Day et al., 2019; Panter and Martin, 2023). For example, Cenozoic lavas from the McMurdo Volcanic Group have $^{3}He/^{4}He$ values from 5.7–7.2R_A, which are quite low to be indicative of a deep, non-degassed plume source (Nardini et al., 2009; Day et al., 2019). Furthermore, despite the presence of a low-velocity thermal anomaly beneath Ross Island (Lloyd et al., 2020), its shallow depth and broad extent (Lloyd et al., 2020) are inconsistent with the dimensions and extent of the deep-sourced plume proposed by Kyle et al. (1992) and other proponents of the plume model (e.g., Phillips et al., 2018).

The alternative hypothesis posits that the CLM source of WARS alkaline volcanism was metasomatized by fluids dehydrated from the Mesozoic Phoenix Plate that was subducted beneath the Gondwana margin. It argues for the creation of metasomes by such slab-derived fluids (i.e., aqueous fluids, silicate melts and/or supercritical silicate-aqueous fluids; Aviado et al., 2015). Fertilization of CLM by LILE-enriched fluids and subsequent radiogenic decay of ^{87}Rb, ^{235}U, ^{238}U, and ^{232}Th could explain the geochemically enriched signature of HIMU-like Sr and Pb isotopic ratios of WARS lavas (Finn et al., 2005; Panter et al., 2006).

In detail, however, the metasomes are most likely not created by typical fluids derived from the subducted Phoenix Plate (Panter et al., 2006, 2018). Plate subduction and concomitant slab-dehydration associated with plate convergence are no longer active during the Cenozoic extension regime whence the alkaline magmas are being generated (Mortimer et al., 2019; Jordan et al., 2020; van de Lagemaat et al., 2022). Also significant is that arc magmas generated from a mantle metasomatized by such aqueous slab-derived fluids are distinctively depleted in high field-strength elements (HFSE), particularly Nb, and enriched in Pb (e.g., Wilson, 1989). In contrast, WARS alkaline lavas are generally enriched in the HFSE or display the so-called positive TITAN (Ti-Ta-Nb) concentration anomaly (Jackson et al., 2007; Peters and Day, 2014) and negative Pb concentration anomaly that are typically possessed by OIB (Fig. 4). Lavas from WARS also exhibit mantle-like or higher Ce/Pb and Nb/U in contrast to the characteristically low Ce/Pb and Nb/U ratios of arc lavas generated from a subduction fluid-metasomatized mantle (Fig. 9c and d; Hofmann et al., 1986). These lavas also do not have the high $^{87}Sr/^{86}Sr$ for given $^{143}Nd/^{144}Nd$ values of arc lavas that are due to the greater mobility of Sr relative to Nd in slab-derived fluids (Zindler and Hart, 1986). Similarly, the heavy $\delta^{18}O$ values of subducting slab materials (e.g., sediments, carbonates, hydrated upper oceanic crust) are not possessed by the WARS samples (Bindeman et al., 2005 and references therein).

As previously discussed, the least-contaminated transect lavas are the primitive ABS alkaline lavas that have a depleted $^{187}Os/^{188}Os_t$ (as low as 0.1254) that trends towards the primitive mantle $^{187}Os/^{188}Os$

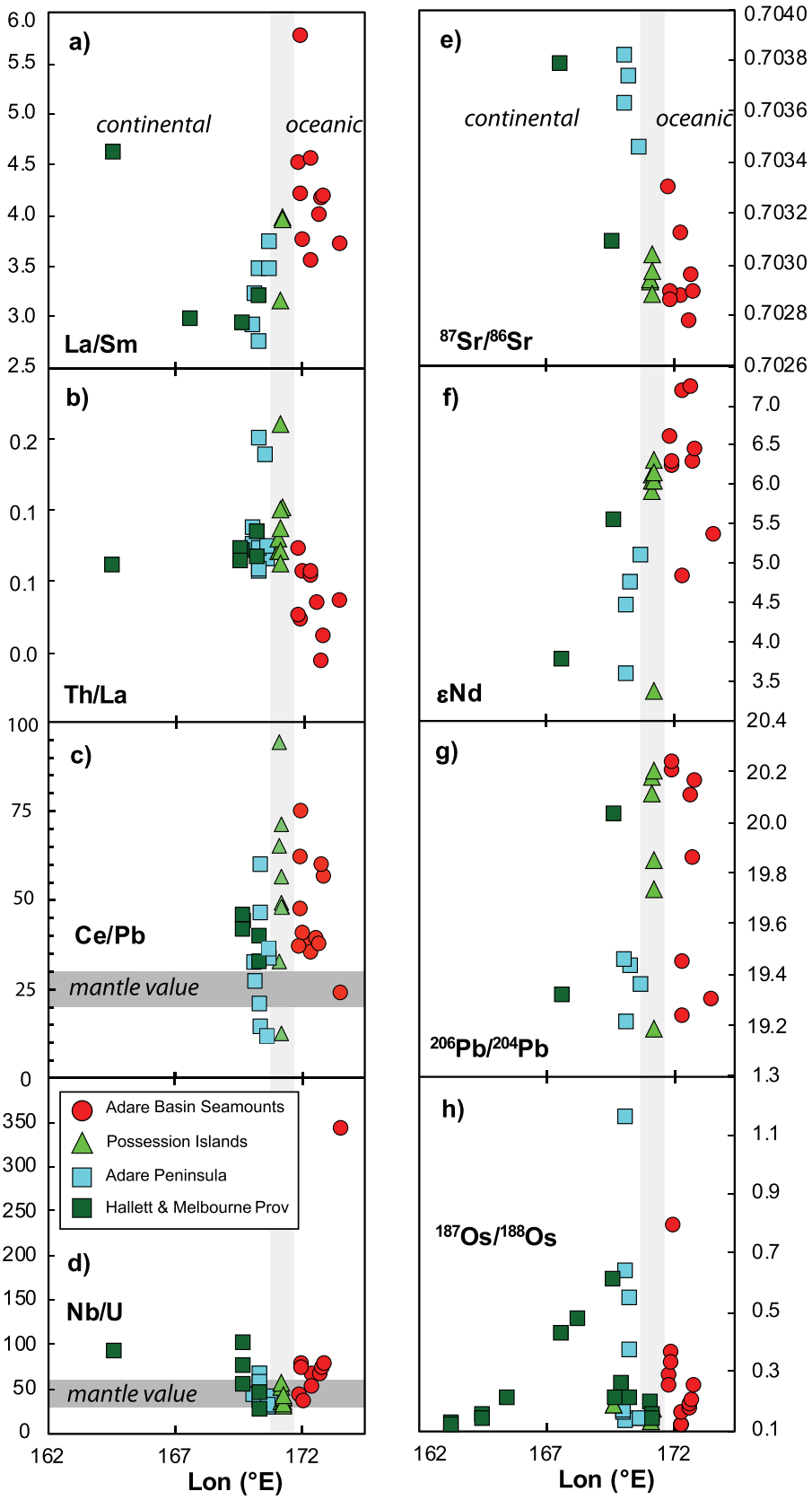

Fig. 9. Various trace element and isotope ratios versus longitude for the northwest Ross Sea lavas. The grey vertical bar represents the oceanic-continental transition zone. Data from Table S1.

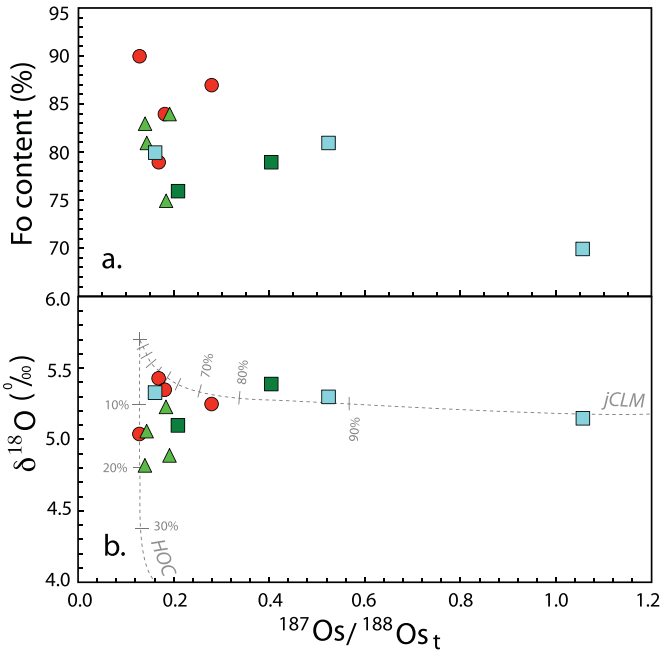

Fig. 10. Age-corrected $^{187}Os/^{188}Os_t$ versus a. forsterite content in olivine and b. $\delta^{18}O$ data measured by SIMS (both from Panter et al., 2018). Shown in b. are mixing models using a primary melt coming from the mantle with Os = 2.0 ppb, $^{187}Os/^{188}Os$ = 0.1296, $\delta^{18}O$ = 5.7 ‰ and O concentration of 40% (Molzahn et al., 1996) and two crustal contaminants: juvenile continental lithospheric mantle (jCLM) with Os = 50 ppt Os; $^{187}Os/^{188}Os$ = 3.5; $\delta^{18}O$ = 5.2 ‰, and O concentration of 48% as inferred from the data and from Molzahn et al. (1996) and a hydrothermally altered oceanic crust (HOC) represented by the altered mugearite sample MB32.11 (Panter et al., 2018) with Os = 10 ppt, $^{187}Os/^{188}Os$ = 3.5, $\delta^{18}O$ = 1.8 ‰ and O concentration of 48%. Symbols as in Fig. 9.

value and modestly radiogenic $^{206}Pb/^{204}Pb$ (up to 20.24; Fig. 8). Their $^{87}Sr/^{86}Sr$ and $^{143}Nd/^{144}Nd$ ratios also indicate a long-time integrated history of geochemical depletion as they plot roughly between the BSE values and the depleted mantle source of MORB (DMM; Fig. 5). Their model mantle source has the compositional features similar to those of FOZO (Panter et al., 2018; Panter and Martin, 2023). The CLM beneath West Antarctica was therefore melt-modified or metasomatized by partial melts originating from previously subducted and already generally dehydrated subducted oceanic slab (Panter et al., 2018; Day et al., 2019). For instance, based on the mixing relationship between basanites and the mantle xenoliths from the Hut Point Peninsula, the radiogenic $^{187}Os/^{188}Os_t$ of the juvenile CLM (Figs. 8 and 10) could be generated through assimilation of pre-existing lithospheric peridotite by melts with high Re/Os (e.g., $^{187}Re/^{188}Os$ = 1305 in sample D7–1; Table 1) in a relatively short period of time (Day et al., 2019). Ultimately, the metasomes in the CLM would be more susceptible to small-degree partial melting due to rifting and/or heat associated with concomitant intraplate volcanism in the Cenozoic (Panter et al., 2018; Day et al., 2019).

The similarity of the mantle source of WARS alkaline lavas to that of alkaline intraplate lavas in the oceanic environment such as oceanic seamount lavas and the global OIB is key to the origin of WARS alkaline magmatism. Alkaline OIB, in particular, most likely come from mantle plumes containing recycled crustal materials that had already gone through subduction dehydration (e.g., Zindler and Hart, 1986; Castillo and Batiza, 1989; Stracke et al., 2005; Hofmann, 2014). The most voluminous component of such recycled material indeed could not have been due to a recent fertilization by subduction-derived fluids as the bulk of OIB are erupted away from active or recently active subduction environments. Instead, FOZO most likely comes from the most voluminous recycled slab material that represents an ancient oceanic lithospheric mantle fertilized through equilibration and remixing (Day et al., 2010), or spiked with subducted marine carbonates that also induce partial melting in the deep mantle (Dasgupta and Hirschmann, 2010; Castillo, 2015).

In our proposed model, the Early Mesozoic Phoenix Plate and its Cretaceous remnants were being subducted beneath the Gondwana margin up until c. 100 Ma (Fig. 11a; Mortimer et al., 2019; van de Lagemaat et al., 2022), generating typical arc magmas (Jordan et al., 2020 and references therein). At this late stage of convergence, most of the arc lavas and the forearc sediments were accreted to the Zealandia Plate above the subducting Hikurangi Plate (e.g., Hoernle et al., 2020; Scott et al., 2021). Plate convergence from the Late Neoproterozoic to Cretaceous (Bradshaw, 1989; Cawood, 2005) also likely placed fragments of the previously subducted oceanic slabs beneath the region (Bredow et al., 2021). The movement of Zealandia away from Gondwana and towards the western Pacific at c. 85 Ma (Fig. 11b) initiated the extension process that includes the formation of the Southern Oceans and, eventually, WARS. The termination of convergence and onset of extension processes were accompanied by a change from arc volcanism erupting sub-alkaline lavas in the Late Cretaceous (Fig. 11a) to intraplate volcanism erupting mostly alkaline OIB-like lavas in the Cenozoic (Figs. 11b and c; Storey et al., 1999; Mukasa and Dalziel, 2000; Hoernle et al., 2020). The FOZO-like signature of alkaline intraplate lavas most likely comes from deep upwellings of small degree partial melts from the fertilized or spiked, previously subducted oceanic lithospheric mantle (or FOZO) beneath the region (Figs. 11b and c) instead of fluids dehydrated from the previously subducted Phoenix Plate (Panter et al., 2006, 2018; Panter and Castillo, 2007; Day et al., 2019) recycled within the mantle wedge (Fig. 11a). The compositional variations of the continent-ocean transect lavas resulted from the interactions of such melts with the juvenile CLM beneath WARS (Panter et al., 2018), which has similar alkaline OIB-like composition as it was generated from a portion of the pre-existing Gondwana lithospheric mantle that was melt-modified (i.e., metasomatized) by similar melts (Day et al., 2019).

6. Implications for other continent-ocean volcanic transects

The alkaline nature and OIB-like isotopic signatures of basalts from the northwestern Ross Sea are, by and large, similar to those of the bulk of lavas from the East African Rift System (EARS) and Cameroon Volcanic Line (CVL) and, therefore, likely linked by a common geologic process. Compared to the WARS, the EARS has >45 Ma of volcanism along structural rifts of various stages of tectonic development and cutting across different geologic terranes amalgamated during the Pan-African Orogeny; these greatly affected the composition of its lavas. To briefly summarize, however, such EARS volcanism has been attributed to either partial melting of the metasomatized CLM due to thermobaric perturbations of the lithosphere or to decompression melting of convecting asthenosphere due to lithospheric thinning (e.g., Rogers, 2006; Furman, 2007; Rooney et al., 2012; Rooney, 2020 and references therein). Some EARS lavas, particularly those from the western branch of the rift system, are clearly contaminated by continental crust. Similar to those in the northwest Ross Sea region of the WARS, however, the bulk of more recent EARS lavas from the more tectonically developed eastern branch of the rift system, save for older ones (Early Miocene) that tend to be more isotopically extreme, are alkaline and OIB-like. Offshore magmatism in southern Mozambique is an extension of that associated with the eastern branch of the EARS (O'Connor et al., 2019). Similar to those in the northwest Ross Sea, proposed models for the source of such EARS alkaline magmas favor hydrated metasomes generated by partial melts from upwelling mantle plumes or by slab-derived fluids during a Neoproterozoic subduction event associated with the Pan-African orogeny (Rooney et al., 2014; Rooney, 2020 and references therein).

Importantly, it has also been suggested that the bulk of EARS alkaline lavas are generated through the long-term (at least, up to c. 500 Myr) metasomatism of the CLM by small-degree partial melts coming from

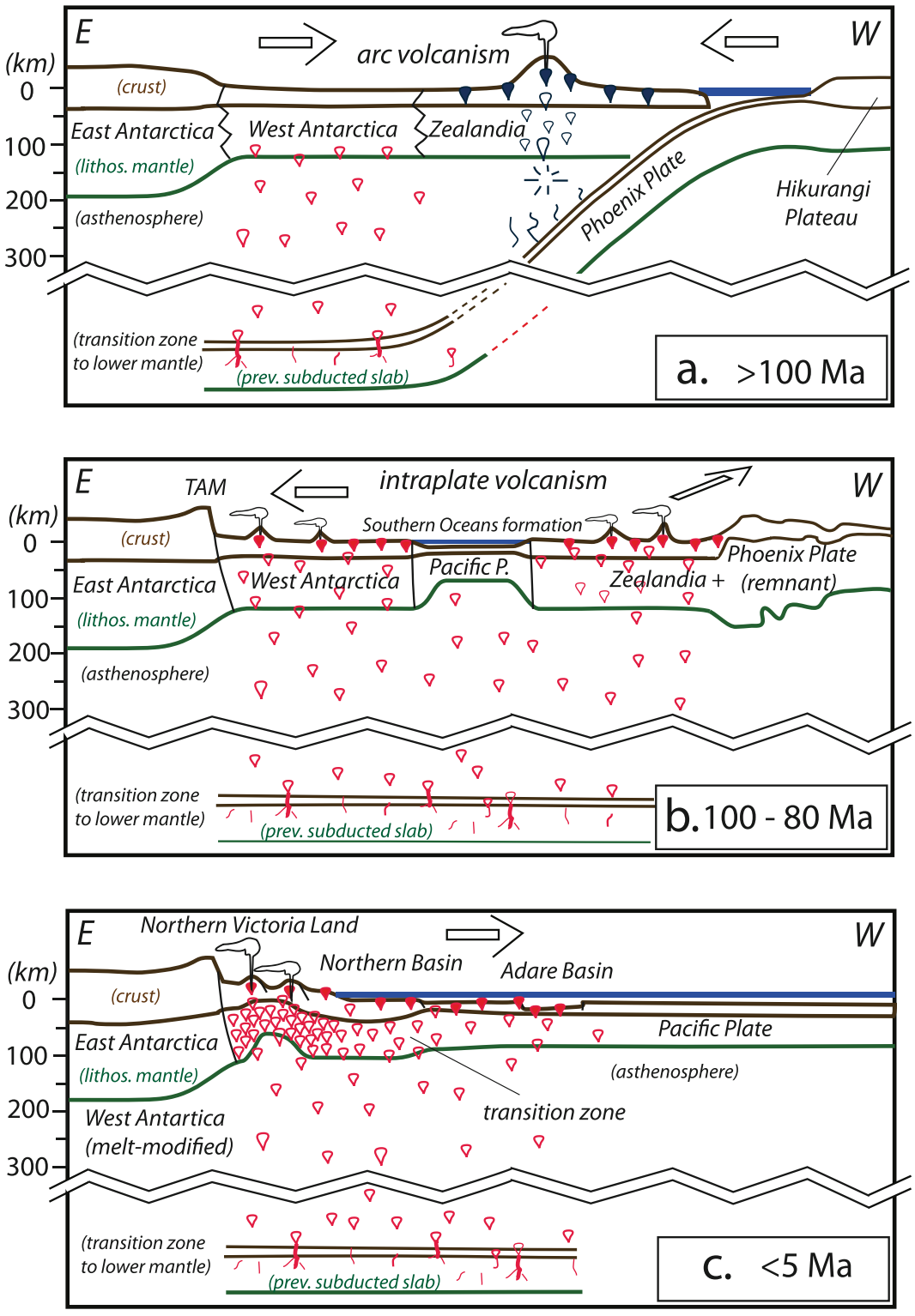

Fig. 11. Schematic illustration of Late Cretaceous to recent tectonism and magmatism in the WARS. (a) Pre-breakup of continental arc. The subduction tectonic regime was nearly continuous from the late Neoproterozoic (c. 550 Ma) to Late Cretaceous (c. 100 Ma) along the Paleo-Pacific margin of Gondwana (e.g., Bradshaw, 1989; Cawood, 2005; Mortimer et al., 2019; van de Lagemaat et al., 2023), generating arc magmatism and providing slab material to the underlying mantle (Bredow et al., 2023). Partial melting of the previously subducted oceanic slab generated small-volume carbonate-rich silicates (Castillo, 2015) that rose, then froze within as well as interacted with the pre-existing continental lithospheric mantle (Panter et al., 2018; Day et al., 2019). (b) Broad regional extension (c. 100 to 80 Ma) of Antarctic continental lithosphere terminated arc magmatism and allowed some of the small-degree partial melts from previously subducted slab to erupt as intraplate lavas; most of the melts continued to modify or re-create the continental lithospheric mantle. Although extension-related intraplate volcanism has been active since the Late Cretaceous, a prominent alkaline igneous activity occurred c. 50 Ma in the WARS (Rocchi et al., 2002) (c) Post-Adare extension. Partial melting in previously subducted oceanic slab continues; those that rise through the continent interact with the melt-modified continental lithosphreric mantle whereas those that rose through the oceanic crust are less contaminated. See additional discussion in the text. (For interpretation of the references to colour in this figure legend, the reader is referred to the web version of this article.)

previously subducted oceanic lithospheric mantle beneath eastern Africa; such melts have a common, FOZO-like composition (Castillo et al., 2014, 2020). The petrogenesis of EARS alkaline magmas, therefore, may be akin to that of northwest Ross Sea alkaline magmas. Unlike in the later, however, the previously subducted oceanic slab beneath the EARS is associated with the Neoproterozoic Pan-African orogeny, more geophysically coherent and connected to the African Large Low Velocity Province (LLVP) centered in the lower mantle beneath southern Africa (Hansen et al., 2012; Castillo et al., 2014, 2020; Rooney, 2020). Notably, the LLVP beneath southern Africa, together with that in south-central Pacific, have been considered as graveyards of subducted oceanic slab (e.g., Hofmann, 2014; Castillo, 2015).

In the CVL case, magmatism consists of a c. 1800 km long linear series of plutonic and volcanic centers from the island of Pagalu through Cameroon and originates from the boundary between the West African and Congo cratons (e.g., Ngwa et al., 2017; Wembenyui et al., 2020 and references therein). The widely accepted model for its origin posits mantle upwelling along a SW-NE 'hot line' due to reactivation of Pan-African lineaments between the cratonic blocks. Repeated motions between the cratons generated low-degree partial melts from the asthenospheric mantle that ponded beneath the lithosphere, but later mixed and metasomatized the compositionally heterogeneous CLM source of CVL lavas. The alternative model that the hotline was created by a mantle plume or series of plumes appear inconsistent with existing data, particularly the lack of systematic volcanic age progression (e.g., Asaah et al., 2015; Ngwa et al., 2017). As a whole, CVL lavas are also alkaline but definitely more compositionally diverse than both EARS and WARS lavas due to variable contributions from EM1, EM2 and DMM mantle end-components (Fig. 5; Asaah et al., 2015 and references therein). Lavas with radiogenic $^{206}Pb/^{204}Pb$ (up to 20.5) indicating a HIMU end-component source also occur in Mount Cameroon although the HIMU-like signature of the lavas diminishes with time (Wembenyui et al., 2020 and references therein). Lavas with a FOZO-like composition are generated through mixing of all the source components (e.g., Asaah et al., 2015). Additionally, some of CVL lavas with low Pb and Nd but high Sr isotopic signature, particularly the Bamoun Plateau lavas, are clearly contaminated by continental crust and/or the CLM beneath western Africa (Atouba et al., 2016; Fig. 5).

Current geophysical models indicate significantly thinner lithosphere beneath the CVL relative to adjacent areas and the low velocity mantle structures beneath the CVL are restricted to the upper mantle (Adams, 2022 and references therein). These have been generally interpreted to support the above notion that the CVL magma source is confined to a hot line in the upper mantle plus CLM and not connected to mantle plumes and/or the deep mantle. However, most recent high-resolution P-wave velocity images of the mantle structure developed using the most extensive collection of travel-time residuals recorded across Africa to date and an adaptive model parameterization show that the CVL magmatism most likely results from the northwestward flow of seismically slow material from the LLVP in southern Africa beneath the Congo Craton (Saeidi et al., 2022). Based on these new geophysical results, therefore, it can be argued that the alkaline lavas in CVL and EARS share a common, subducted oceanic lithospheric mantle source and that the enhanced compositional diversity of CVL lavas is simply due to the inefficacies of mixing among the various source components from the LLVP and CLM beneath western Africa. Thus, it is possible that the alkaline magmas in northwest Ross Sea, EARS and CVL have commonalities in their origins; their compositional variations represent the diversity of melts coming from different periods and stages of recycling of previously subducted oceanic slab and interactions of such melts with the overlying asthenosphere and continental lithosphere.

7. Conclusions

Results of this study indicate that the primary alkaline magmas of continental-oceanic transect lavas in the northwest Ross Sea region can be best inferred from primitive oceanic lavas; they come from upwelling small degree partial melts with characteristic features of the FOZO mantle component. Such a component most likely originates from previously subducted oceanic lithospheric mantle. The new *Re*—Os and HSE abundance data clearly suggest that contamination by continental lithospheric mantle is an ancillary process that strongly affects partial melts infiltrating the thicker continental lithosphere, and is largely responsible for creating the continental-oceanic geochemical trends of the transect lavas. Furthermore, the compositional similarities among the northwest Ross Sea, CVL and EARS continent-oceanic transect lavas, particularly their alkaline nature and OIB-like isotopic signatures, are most likely linked by a common geologic process.

Declaration of Competing Interest

The authors declare that they have no known competing financial interests or personal relationships that could have appeared to influence the work reported in this paper.

Data availability

All data are available in the text and supplementary material.

Acknowledgments

This work was funded by National Science Foundation grants (NSF-1333698; EAR-1918322) to P. Castillo and J. Day. We sincerely thank N. Juda for assistance in the analysis, the two anonymous reviewers for their detailed and constructive comments that greatly improve the manuscript and S. Aulbach for excellent editorial handling.

Appendix A. Supplementary data

Supplementary data to this article can be found online at https://doi.org/10.1016/j.chemgeo.2023.121780.

References

Adams, A., 2022. Insights into the source of magmatic hot-lines: forty years of geophysical studies of the Cameroon Volcanic Line. Front. Earth Sci. 10 https://doi.org/10.3389/feart.2022.838993.

Antibus, J.V., Panter, K.S., Wilch, T.I., Dunbar, N., McIntosh, W., Tripati, A., Bindeman, I., Blusztajn, J., 2014. Alteration of volcaniclastic deposits at Minna Bluff: geochemical insights on mineralizing environment and climate during the Late Miocene in Antarctica. Geochem. Geophys. Geosyst. 15, 3258–3280.

Armienti, P., Francalanci, L., Landi, P., Vita, G., Zone, 2003. In: Tessensohn, F., Ricci, C. A. (Eds.), Geol. Jahr. Polar Issue 9, 409–445.

Armienti, P., Perinelli, C., 2010. Cenozoic thermal evolution of lithospheric mantle in northern Victoria Land (Antarctica): evidences from mantle xenoliths. Tectonophysics 486, 28–35.

Armstrong, R.L., 1978. K-Ar dating: Late Cenozoic McMurdo Volcanic Group and dry valley glacial history, Victoria Land, Antarctica. N Z. J. Geol. Geophys. 21, 685–698.

Asaah, A.N.E., Yokoyama, T., Aka, F.T., Usui, T., Wirmvem, M.J., Tchamabe, B.C., Ohba, T., Tanyileke, G., Hell, J.V., 2015. A comparative review of petrogenetic processes beneath the Cameroon Volcanic Line: geochemical constraints. Geosci. Front. 6, 557–570.

Atouba, L.C.O., Chazot, G., Moundi, A., Agranier, A., Bellon, H., Nonnotte, P., Nzenti, J.-P., Kankeu, B., 2016. Mantle sources beneath the Cameroon Volcanic Line: geochemistry and geochronology of the Bamoun plateau mafic rocks. Arab. J. Geosci. 9, 270. https://doi.org/10.1007/s12517-015-2285-6.

Aviado, K.B., Rilling-Hall, S., Bryce, J.G., Mukasa, S.B., 2015. Submarine and subaerial lavas in the West Antarctic Rift System: temporal record of shifting magma source components from the lithosphere and asthenosphere. Geochem. Geophys. Geosyst. 16, 4344–4361.

Bindenman, I.N., Eiler, J.M., Yogodzinski, G.M., Tatsumi, Y., Stern, C.R., Grove, T.L., Portnyagin, M., Hoernle, K., Danyushevsky, L.V., 2005. Oxygen isotope evidence for slab melting in modern and ancient subduction zones. Earth Planet. Sci. Lett. 235, 480–496.

Birck, J.L., Barman, M.R., Capmas, F., 1997. Re-Os isotopic measurements at the femtomole level in natural samples. Geostand. Geoanal. Res. 20, 19–27.

Boger, S.D., Miller, J.M.L., 2004. Terminal suturing of Gondwana and the onset of the Ross-Delamerian Orogeny: the cause and effect of an Early Cambrian reconfiguration of plate motions. Earth Planet. Sci. Lett. 219, 35–48.

Borg, S.G., Stump, E., 1987. Paleozoic magmatism and associated tectonic problems of Northern Victoria Land, Antarctica. Gondwana six: structure, tectonics, and geophysics. Geophys. Monogr. 40, 67–75.
Bradshaw, J.D., 1989. Cretaceous geotectonic patterns in the New Zealand region. Tectonics 8, 803–820.
Bredow, E., Steinberger, B., Gassmöller, R., Dannberg, J., 2021. Mantle convection and possible mantle plumes beneath Antarctica – Insights from geodynamic models and implications for topography. In: Martin, A.P., van der Wal, W. (Eds.), The Geochemistry and Geophysics of the Antarctic Mantle. Geological Society, London, Memoir 56. https://doi.org/10.1144/M56-2020-2.
Cande, S.C., Stock, J.M., 2006. Constraints on the timing of Extension in the Northern Basin, Ross Sea. In: Fütterer, D.K., Damaske, D., Kleinschmidt, G., Miller, H., Tessensohn, F. (Eds.), Antarctica. Springer, Berlin Heidelberg, Berlin, Heidelberg, pp. 319–326.
Cande, S.C., Stock, J.M., Müller, R.D., Ishihara, T., 2000. Cenozoic motion between east and West Antarctica. Nature 404, 145–150.
Castillo, P.R., 2015. The recycling of marine carbonates and sources of HIMU and FOZO Ocean island basalts. Lithos 216–217, 254–263.
Castillo, P.R., Batiza, R., 1989. Strontium, Neodymium, and lead isotope constraints on near ridge seamount production beneath the South Atlantic. Nature 342, 262–265.
Castillo, P.R., Hilton, D.R., Halldorsson, S.A., 2014. Trace element and Sr-Nd-Pb isotope geochemistry of Rungwe Volcanic Province, Tanzania: implications for a superplume source for East Africa Rift magmatism. Front. Earth Sci. https://doi.org/10.3389/feart.2014.00021.
Castillo, P.R., Liu, X., Scarsi, P., 2020. The geochemistry and Sr-Nd-Pb isotopic ratios of high $^{3}He/^{4}He$ Afar and MER basalts indicate a significant role of the African Superplume in EARS magmatism. Lithos 376-377, 105791. https://doi.org/10.1016/j.lithos.2020.105791.
Cawood, P.A., 2005. Terra Australis Orogen: Rodinia breakup and development of the Pacific and Iapetus margins of Gondwana during the Neoproterozoic and Paleozoic. Earth Sci. Rev. 69, 249–279.
Cohen, A.S., Waters, F.G., 1996. Separation of osmium from geological materials by solvent extraction for analysis by thermal ionisation mass spectrometry. Anal. Chim. Acta 332, 269–275.
Craig, H., 1961. Isotopic variations in meteoric water. Science 133, 1702–1703.
Dasgupta, R., Hirschmann, M.M., 2010. The deep carbon cycle and melting in Earth's interior. Earth Planet. Sci. Lett. 298, 1–13.
Davey, F.J., Brancolini, G., 1995. The Late Mesozoic and Cenozoic Structural Setting of the Ross Sea Region. Geology and Seismic Stratigraphy of the Antarctic Margin, 68, pp. 167–182.
Davey, F.J., Cande, S.C., Stock, J.M., 2006. Extension in the western Ross Sea region-links between Adare Basin and Victoria Land Basin. Geophys. Res. Lett. 33, 1–5.
Davy, B., Hoernle, K., Werner, R., 2008. Hikurangi Plateau: crustal structure, rifted formation, and Gondwana subduction history. Geochem. Geophys. Geosyst. 9 (7).
Day, J.M.D., 2013. Hotspot volcanism and highly siderophile elements. Chem. Geol. 341, 50–74.
Day, J.M.D., Pearson, D.G., Macpherson, C.G., Lowry, D., Carracedo, J.-C., 2010. Evidence for distinct proportions of subducted oceanic crust and lithosphere in HIMU-type mantle beneath El Hierro and La Palma, Canary Islands. Geochim. Cosmochim. Acta 74, 6565–6589.
Day, J.M.D., Peters, B.J., Janney, P.E., 2014. Oxygen isotope systematics of South African olivine melilitites and implications for HIMU mantle reservoirs. Lithos 202-203, 76–84.
Day, J.M.D., Waters, C.L., Schaefer, B.F., Walker, R.J., Turner, S., 2016. Use of hydrofluoric acid desilicification in the determination of highly siderophile element abundances and Re-Pt-Os isotope systematics in mafic-ultramafic rocks. Geostand. Geoanal. Res. 40, 49–65.
Day, J.M.D., Walker, R.J., Warren, J.M., 2017. ^{186}Os–^{187}Os and highly siderophile element abundance systematics of the mantle revealed by abyssal peridotites and Os-rich alloys. Geochim. Cosmochim. Acta 200, 232–254.
Day, J.M.D., Harvey, R.P., Hilton, D.R., 2019. Melt-modified lithosphere beneath Ross Island and its role in the tectono-magmatic evolution of the West Antarctic Rift System. Chem. Geol. 518, 45–54.
Day, J.M.D., Nutt, K.L., Mendenhall, B., Peters, B.J., 2021. Temporally variable crustal contributions to primitive mantle-derived Columbia River Basalt Group magmas. Chem. Geol. 572, 120–197.
Day, J.M.D., Troll, V.R., Aulinas, M., Deegan, F., Geiger, H., Carracedo, J.C., Gisbert Pinto, G., Perez Torrado, F.J., 2022. Mantle source characteristics and magmatic processes during the 2021 La Palma eruption. Earth Planet. Sci. Lett. 597, 117793.
Di Vincenzo, G., Horton, F., Palmeri, R., 2016. Protracted (~ 30 Ma) eclogite-facies metamorphism in northern Victoria Land (Antarctica): implications for the geodynamics of the Ross/Delamerian Orogen. Gondwana Res. 40, 91–106.
Esser, R., Kyle, P.R., 2002. 40Ar/39Ar chronology the McMurdo Volcanic Group at the Pleiades, northern Victoria Land, Antarctica. Proc. R. Soc. N. Z. Bull. 35, 415–418.
Faccenna, C., Rossetti, F., Becker, T.W., Danesi, S., Morelli, A., 2008. Recent extension driven by mantle upwelling beneath the Admiralty Mountains (East Antarctica). Tectonics 27 (4).
Finn, C.A., Müller, R.D., Panter, K.S., 2005. A Cenozoic diffuse alkaline magmatic province (DAMP) in the Southwest Pacific without rift or plume origin. Geochem. Geophys. Geosyst. 6 https://doi.org/10.1029/2004GC000723.
Fitton, J.G., Dunlop, H.M., 1985. The Cameroon line, West Africa, and its bearing on the origin of oceanic and continental alkali basalt. Earth Planet. Sci. Lett. 72, 23–38.
Furman, T., 2007. Geochemistry of East African Rift basalts: an overview. J. Afr. Earth Sci. 48, 147–160.
Gonfiantini, R., Picciotto, E., 1959. Oxygen isotope variations in Antarctic snow samples. Nature 184, 1557–1558.
Granot, R., Cande, S.C., Stock, J.M., Davey, F.J., Clayton, R.W., 2010. Postspreading rifting in the Adare Basin, Antarctica: regional tectonic consequences. Geochem. Geophys. Geosyst. 11, 1–29.
Granot, R., Cande, S.C., Stock, J.M., Damaske, D., 2013. Revised Eocene-Oligocene kinematics for the West Antarctic rift system. Geophys. Res. Lett. 40, 279–284.
Hanan, B.B., Graham, D.W., 1996. Lead and helium isotope evidence from oceanic basalts for a common deep source of mantle plumes. Science 272, 991–995.
Hansen, S.E., Nyblade, A.A., Benoit, M.H., 2012. Mantle structure beneath Africa and Arabia from adaptively parameterized P-wave tomography: implications for the origin of Cenozoic Afro-Arabian tectonism. Earth Planet. Sci. Lett. 319-320, 23–34.
Hart, S.R., Hauri, E.H., Oschman, L.A., Whitehead, J.A., 1992. Mantle plumes and entrainment: the isotopic evidence. Science 256, 517–520.
Hart, S.R., Blusztajn, J., LeMasurier, W.E., Rex, D.C., 1997. Hobbs Coast Cenozoic volcanism: implications for the West Antarctic rift system. Chem. Geol. 139, 223–248.
Hauri, E.H., Whitehead, J.A., Hart, S.R., 1994. Fluid dynamic and geochemical aspects of entrainment in mantle plumes. J. Geophys. Res. Solid Earth 99, 24275.
Hoernle, K., Timm, C., Hauff, F., Tappenden, V., Werner, R., Jolis, E.M., Mortimer, N., Weaver, S., Riefstahl, F., Gohl, K., 2020. Late Cretaceous (99-69 Ma) basaltic intraplate volcanism on and around Zealandia: tracing upper mantle geodynamics from Hikurangi Plateau collision to Gondwana breakup and beyond. Earth Planet. Sci. Lett. 529, 115–864.
Hofmann, A.W., 2014. Sampling mantle heterogeneity through oceanic basalts: Isotopes and trace elements. In: Treatise on Geochemistry, , 2nd ed.vol. 3. Elsevier, pp. 67–101.
Hofmann, A.W., Jochum, K.P., Seufert, M., White, W.M., 1986. Nb and Pb in oceanic basalts: new constraints on mantle evolution. Earth Planet. Sci. Lett. 79, 33–45.
Hole, M.J., 1988. Post-subduction alkaline volcanism along the Antarctic Peninsula. J. Geol. Soc. Lond. 145, 985–988.
Huerta, A.D., Harry, D.L., 2007. The transition from diffuse to focused extension: modeled evolution of the West Antarctic Rift system. Earth Planet. Sci. Lett. 255, 133–147.
Jackson, M.G., Hart, S.R., Koppers, A.A.P., Staudigel, H., Konter, J., Blusztajn, J., Kurz, M., Russell, J.A., 2007. The return of subducted continental crust in Samoan lavas. Nature 448, 684–687.
Janney, P.E., Castillo, P.R., 1996. Basalts from the Central Pacific Basin: evidence for the origin of cretaceous igneous complexes in the Jurassic western Pacific. J. Geophys. Res. 101, 2875–2893.
Ji, F., Li, F., Gao, J.Y., Zhang, Q., Hao, W.F., 2018. 3-D density structure of the Ross Sea basins, West Antarctica from constrained gravity inversion and their tectonic implications. Geophys. J. Int. 215, 1241–1256.
Johnson, D.M., Hooper, P.R., Conrey, R.M., 1999. XRF Analysis of rocks and minerals for major and trace elements on a single low dilution Li-tetraborate fused bead. Adv. X-ray Anal. 41, 843–867.
Jordan, T.A., Riley, T.R., Siddoway, C.S., 2020. The geological history and evolution of West Antarctica. Nat. Rev. Earth Environ. 1, 117–133.
Kellogg, T.B., Kellogg, D.E., Stuiver, M., 1991. Oxygen isotope data from the McMurdo Ice Shelf, Antarctica: implications for debris band formation and glacial history. Antarctic J. US 26, 73–76.
King, E.M., Valley, J.W., Davis, D.W., Edwards, G.R., 1998. Oxygen isotope ratios of Archean plutonic zircons from granite-greenstone belts of the Superior Province: indicator of magmatic source. Precambrian Res. 92, 365–387.
Kipf, A., Hauff, F., Werner, R., Gohl, K., van den Bogaard, P., Hoernle, K., Maicher, D., Klügel, A., 2014. Seamounts off the West Antarctic margin: a case for non-hotspot driven intraplate volcanism. Gondwana Res. 25, 1660–1679.
Košler, J., Magna, T., Mlcoch, B., Mixa, P., Nyvlt, D., Holub, F.V., 2009. Combined Sr, Nd, Pb and Li isotope geochemistry of alkaline lavas from northern James Ross Island (Antarctic Peninsula) and implications for back-arc magma formation. Chem. Geol. 258, 207–218.
Kyle, P.R., McIntosh, W.C., Schmidt-Thomé, M., Mueller, P., Tessensohn, F., Noll, M.R., Wörner, G., Wörner, G., Viereck, L., Behrendt, J.C., Ellerman, P.J., Wright, A.C., Moore, J.A., Stump, E., Borg, S.G., Sheridan, M.F., 1990. A. McMurdo Volcanic Group Western Ross embayment. In: LeMasurier, W.E., Thomson, J.W., Baker, P.E., Kyle, P.R., Rowley, P.D., Smellie, J.L., Verwoerd, W.J. (Eds.), Volcanoes of the Antarctic Plate and Southern Oceans, pp. 18–145.
Kyle, P.R., Moore, J.A., Thirlwall, M.F., 1992. Petrologic Evolution of Anorthoclase Phonolite Lavas at Mount Erebus, Ross Island, Antarctica. J. Petrol. 33, 849–875.
Langmuir, C.H., Vocke, R.D., Hanson, G.N., Hart, S.R., 1978. A general mixing equation with applications to Icelandic basalts. Earth Planet. Sci. Lett. 37, 380–392.
Lanyon, R., Varne, R., Crawford, A.J., 1993. Tasmanian Tertiary basalts, the Balleny Plume, and opening of the Tasman Sea Southwest Pacific Ocean. Geology 21, 555–558.
Lawrence, J.F., Wiens, D.A., Nyblade, A.A., Anandakrishan, S., Shore, P.J., Voigt, D., 2006. Upper mantle thermal variations beneath the Transantarctic Mountains inferred from teleseismic S-wave attenuation. Geophys. Res. Lett. 33, 2–5.
Le Bas, M.J., Le Maitre, R.W., Streckeisen, A., Zanettin, B., 1986. A chemical classification of volcanic rocks based on the total alkali silica diagram. J. Petrol. 27, 745–750.
LeMasurier, W.E., Rex, D.C., 1991. The Marie Byrd Land volcanic province and its relation to the Cainozoic West Antarctic rift system. In: Tingey, R.J. (Ed.), The Geology of Antarctica, pp. 249–284.
Li, J., Liang, X.R., Xu, J.F., Suzuki, K., Dong, Y.H., 2010. Simplified technique for the measurements of Re-Os isotope by multicollector inductively coupled plasma mass spectrometry (MC-ICP-MS). Geochem. J. 44, 73–80.

Li, J., Jiang, X., Xu, J., Zhong, L., 2014. Determination of platinum-group elements and Re-Os isotopes using ID-ICP-MS and N-TIMS from a single digestion after two-stage column separation. Geostand. Geoanal. Res. 38, 37–50.
Lloyd, A.J., Wiens, D.A., Zhu, H., Tromp, J., Nyblade, A.A., Aster, R.C., Hansen, S.E., Dalziel, I.W., Wilson, T.J., Ivins, E.R., O'Donnell, J.P., 2020. Seismic structure of the Antarctic upper mantle imaged with adjoint tomography. J. Geophys. Res. Solid Earth 125 (3).
Luyendyk, B.P., 1995. Hypothesis for Cretaceous rifting of east Gondwana caused by subducted slab capture. Geology 23, 373–376.
Macdonald, G.A., Katsura, T., 1964. Chemical composition of Hawaiian lavas. J. Petrol. 5, 82–133.
Martin, A.P., Cooper, A.F., Price, R.C., 2013. Petrogenesis of Cenozoic, alkalic volcanic lineages at Mount Morning, West Antarctica and their entrained lithospheric mantle xenoliths: lithospheric versus asthenospheric mantle sources. Geochim. Cosmochim. Acta 122, 127–152.
Martin, A.P., Cooper, A.F., Price, R.C., Kyle, P.R., Gamble, J.A., 2021. Chapter 5.2 b Erebus Volcanic Province: petrology. Geol. Soc. Lond. Mem. 55, 447–489.
Mattey, D., Lowry, D., Macpherson, C., 1994. Oxygen isotope composition of mantle peridotite. Earth Planet. Sci. Lett. 128, 231–241.
McDonough, W.F., Sun, S.S., 1995. The composition of the Earth. Chem. Geol. 120, 223–253.
Meisel, T., Mosser, J., 2004. Platinum-group elements and rhenium concentrations in low abundance reference materials. Geostand. Geoanal. Res. 28, 233–250.
Meisel, T., Walker, R.J., Irving, A.J., Lorand, J.P., 2001. Osmium isotopic compositions of mantle xenoliths: a global perspective. Geochim. Cosmochim. Acta 65, 1311–1323.
Merle, R.E., Jiang, Q., Jourdan, F., Olierook, H., 2022. The age and origin of the Balleny and Scott volcanic provinces, Ross Sea, Antarctica. Geochemistry 82, 125904. https://doi.org/10.1016/j.chemer.2022.125904.
Molzahn, M., Reisberg, L., Wiirner, G., 1996. OS, Sr, Nd, Pb, 0 isotope and trace element data from the Ferrar flood basalts, Antarctica: evidence for an enriched subcontinental lithospheric source. Earth Planet. Sci. Lett. 144, 529–546.
Mortimer, N., Dunlap, W.J., Isaac, M.J., Sutherland, R.P., Faure, K., 2007. Basal Adare volcanics. Robertson Bay, North Victoria Land, Antarctica: late Miocene intraplate basalts of subaqueous origin. In: Cooper, A.K., Raymond, C.R., et al. (Eds.), p. 7.
Mortimer, N., van den Bogaard, P., Hoernle, K., Timm, C., Gans, P.B., Werner, R., Riefstahl, F., 2019. Late Cretaceous oceanic plate reorganization and the breakup of Zealandia and Gondwana. Gondwana Res. 65, 31–42.
Muehlenbachs, K., Anderson Jr., A.T., Sigvaldason, G.E., 1974. Low-^{18}O basalts from Iceland. Geochim. Cosmochim. Acta 38, 577–588.
Mukasa, S.B., Dalziel, I.W., 2000. Marie Byrd Land, West Antarctica: evolution of Gondwana's Pacific margin constrained by zircon U-Pb geochronology and feldspar common-Pb isotopic compositions. Geol. Soc. Am. Bull. 112, 611–627.
Muller, P., Schmidt-Thome, M., Kreuzer, H., Tessesohn, H., Vetter, U., 1991. Cenozoic peralkaline magmatism at the western margin of the Ross Sea, Antarctica. Memorie della Societie Geologica Italiana 46, 315–336.
Nardini, I., Armienti, P., Rocchi, S., Dallai, L., Harrison, D., 2009. Sr-Nd-Pb-He-O isotope and geochemical constraints on the genesis of cenozoic magmas from the West Antarctic Rift. J. Petrol. 50, 1359–1375.
Ngwa, C.N., Hansteen, T.H., Devey, C.W., van der Zwan, F.M., Suh, C.E., 2017. Origin and evolution of primitive melts from the Debunscha Maar, Cameroon: consequences for mantle source heterogeneity within the Cameroon Volcanic Line. Lithos 288–289, 326–337.
O'Connor, J.M., Jokat, W., Regelous, M., Kuiper, K.F., Miggins, D.P., Koppers, A.A.P., 2019. Superplume mantle tracked isotopically the length of Africa from the Indian Ocean to the Red Sea. Nat. Commun. 10, 5493. https://doi.org/10.1038/s41467-19-13181-7.
Panter, K.S., 2021. Chapter 1.3 Antarctic volcanism: petrology and tectonomagmatic overview. Geol. Soc. Lond. Mem. 55, 43–53.
Panter, K.S., Castillo, P., 2007. Petrogenesis and source of lavas from seamounts in the Adare Basin, western Ross Sea; implications for the origin of Cenozoic magmatism in Antarctica. In: Open-File Report - U. S. Geological Survey Extended Abstract 069..
Panter, K.S., Martin, A.P., 2023. West Antarctic mantle deduced from mafic magmatism. Geol. Soc. Lond. Mem. 56, 133–149.
Panter, K.S., Hart, S.R., Kyle, P., Blusztanjn, J., Wilch, T., 2000. Geochemistry of Late Cenozoic basalts from the Crary Mountains: characterization of mantle sources in Marie Byrd Land, Antarctica. Chem. Geol. 165, 215–241.
Panter, K.S., Blusztajn, J., Hart, S.R., Kyle, P.R., Esser, R., McIntosh, W.C., 2006. The origin of HIMU in the SW Pacific: evidence from intraplate volcanism in southern New Zealand and subantarctic islands. J. Petrol. 47, 1673–1704.
Panter, K.S., Castillo, P.R., Krans, S., Deering, C., McIntosh, W., Valley, J.W., Kitajima, K., Kyle, P.R., Hart, S.R., Blusztajn, J., 2018. Melt origin across a rifted continental margin: a case for subduction-related metasomatic agents in the lithospheric source of alkaline basalt, NW Ross Sea, Antarctica. J. Petrol. 59, 517–558.
Panter, K.S., Wilch, T.I., Smellie, J.L., Kyle, P.R., McIntosh, W.C., 2021. Chapter 5.4 b Marie Byrd Land and Ellsworth Land: petrology. Geol. Soc. Lond. Mem. 55, 577–614.
Panter, K.S., Castillo, P., Krans, S., Deering, C., McIntosh, W., Valley, J., Kitajima, K., Kyle, P., Hart, S., Blusztajn, J., 2023. Erratum. correction to: melt origin across a rifted continental margin: a case for subduction-related metasomatic agents in the lithospheric source of alkaline basalt, NW Ross Sea, Antarctica. J. Petrol. 64 https://doi.org/10.1093/petrology/egad017 egad017.
Peters, B.J., Day, J.M.D., 2014. Assessment of relative Ti, Ta and Nb (TITAN) enrichments in ocean island basalts. Geochem. Geophys. Geosyst. 4424–4444.
Peucker-Ehrenbrink, B., Bach, W., Hart, S.R., Blusztajn, J.S., Abbruzzese, T., 2003. Rhenium-osmium isotope systematics and platinum group element concentrations in oceanic crust from DSDP/ODP Sites 504 and 417/418. Geochem. Geophys. Geosyst. 4, 8911. https://doi.org/10.1029/2002GC000414.
Phillips, E.H., Sims, K.W.W., Blichert-Toft, J., Aster, R.C., Gaetani, G.A., Kyle, P.R., Wallace, P.J., Rasmussen, D.J., 2018. The nature and evolution of mantle upwelling at Ross Island, Antarctica, with implications for the source of HIMU lavas. Earth Planet. Sci. Lett. 498, 38–53.
Risk, G.F., Hochstein, M.P., 1974. Heat flow at arrival heights, Ross Island, Antarctica. N. Z. J. Geol. Geophys. 17, 629–644.
Rocchi, S., Smellie, J.L., 2021. Chapter 5.1 b Northern Victoria Land: petrology. Geol. Soc. Lond. Mem. 55, 383–413.
Rocchi, S., Armienti, P., D'Orazio, M., Tonarini, S., Wijbrans, J.R., Di Vincenzo, G., 2002. Cenozoic magmatism in the western Ross Embayment: Role of mantle plume versus plate dynamics in the development of the West Antarctic Rift System. J. Geophys. Res. Solid Earth 107, ECV-5.
Rocholl, A., Stein, M., Molzahan, M., Hart, S.R., Worner, G., 1995. Geochemical evolution of rift magmas by progressive tapping of a stratified mantle source beneath the Ross Sea rift, Northern Victoria Land, Antarctica. Earth Planet. Sci. Lett. 131, 207–224.
Rogers, N.W., 2006. Basaltic magmatism and the geodynamics of the East African Rift System. Geol. Soc. Lond., Spec. Publ. 259, 77. https://doi.org/10.1144/GSL.SP.2006.259.01.08.
Rooney, T.O., 2020. The Cenozoic magmatism of East Africa: part V–magma sources and processes in the East African Rift. Lithos 360, 105296.
Rooney, T.O., Hanan, B.B., Graham, D.W., Furman, T., Blichert-Toft, J., Schilling, J.-G., 2012. Upper mantle pollution during Afar plume–continental rift interaction. J. Petrol. 53, 365–389.
Rooney, T.O., Nelson, W.R., Dosso, L., Furman, T., Hannan, B., 2014. The role of continental lithosphere metasomes in the production of HIMU-like magmatism on the northeast African and Arabian plates. Geology 42, 419–422.
Rudnick, R.L., Gao, S., 2014. Composition of the continenetal crust. In: Treatise on Geochemistry 2nd Edition. https://doi.org/10.1016/B978-0-08-095975-7.00301-6 1.
Saeidi, H., Hansen, S.E., Nyblad, A.A., 2022. Deep mantle influence on the Cameroon Volcanic Line. Geochem. Geophys. Geosyst. 24 https://doi.org/10.1029/2022GC010621 e2022GC010621.
Salters, V.J.M., Sachi-Kocher, A., 2010. An ancient metasomatic source for the Walvis Ridge basalts. Chem. Geol. 273, 151–167.
Salvini, F., Brancolini, G., Busetti, M., Storti, F., Mazzarini, F., Coren, F., 1997. Cenozoic geodynamics of the Ross Sea region, Antarctica: crustal extension, intraplate strike-slip faulting, and tectonic inheritance. J. Geophys. Res. Solid Earth 102, 24669–24696. https://doi.org/10.1029/97jb01643.
Scott, J.M., Pearson, D.G., Liu, J., Auer, A., Cooper, A.F., Li, D., Palmer, M.C., Read, S.E., Reid, M.R., Woodland, S.J., 2021. Osmium isotopes in peridotite xenoliths reveal major mid-Proterozoic lithosphere formation under the Transantarctic Mountains. Geochm. Cosmochim. Acta 312, 25–43.
Sims, K.W.W., Blichert-Toft, J., Kyle, P.R., Pichat, S., Gauthier, P.-J., Blusztajn, J., Kelly, P., Ball, L., Layne, G., 2008. A Sr, Nd, Hf, and Pb isotope perspective on the genesis and long-term evolution of alkaline magmas from Erebus volcano, Antarctica. J. Volcanol. Geotherm. Res. 177, 606–618.
Smellie, J.L., Martin, A.P., 2021. Chapter 5.2 a Erebus Volcanic Province: volcanology. Geol. Soc. Lond. Mem. 55, 415–446.
Smellie, J.L., Rocchi, S., 2021. Chapter 5.1 a Northern Victoria Land: volcanology. Geol. Soc. Lond. Mem. 55, 347–381.
Smellie, J.L., Rocchi, S., Armienti, P., 2011. Late Miocene volcanic sequences in northern Victoria Land, Antarctica: products of glaciovolcanic eruptions under different thermal regimes. Bull. Volcanol. 73, 1–25.
Stewart, M.K., 1975. Hydrogen and oxygen isotope studies on the McMurdo ice shelf, Antarctica. N. Z. J. Geol. Geophys. 18, 49–64.
Storey, B.C., Leat, P.T., Weaver, S.D., Pankhurst, R.J., Bradshaw, J.D., Kelley, S., 1999. Mantle plumes and Antarctica-New Zealand rifting: evidence from mid-cretaceous mafic dykes. J. Geol. Soc. 156, 659–671.
Stracke, A., Bizimis, M., Salters, V.J.M., 2003. Recycling oceanic crust: Quantitative constraints. Geochem. Geophys. Geosyst. 4 https://doi.org/10.1029/2001GC000223.
Stracke, A., Hofmann, A.W., Hart, S.R., 2005. FOZO, HIMU, and the rest of the mantle zoo. Geochem. Geophys. Geosyst. 6 https://doi.org/10.1029/2004GC000824.
Sun, S.-S., McDonough, W.F., 1989. Chemical and isotopic systematics of oceanic basalts: implications for mantle composition and processes. Geol. Soc. Lond., Spec. Publ. 42, 313–345.
Thirlwall, M.F., 1997. Pb isotopic and elemental evidence for OIB derivation from young HIMU mantle. Chem. Geol. 139, 51–74.
van de Lagemaat, S.H., Kamp, P.J., Boschman, L.M., Van Hinsbergen, D.J., 2022. Reconciling the Cretaceous breakup and demise of the Phoenix Plate with East Gondwana orogenesis in New Zealand. Earth Sci. Rev. 104276.
Weaver, S.D., Storey, B.C., Pankhurst, R.J., Mukasa, S.B., DiVenere, V.J., Bradshaw, J.D., 1994. Antarctic–New Zealand rifting and Marie Byrd Land lithospheric magmatism linked to ridge subduction and mantle plume activity. Geology 22, 811–814.
Wembenyui, E.W., Collerson, K.D., Zhao, J. Xin, 2020. Evolution of Mount Cameroon volcanism: geochemistry, mineral chemistry and radiogenic isotopes (Pb, Sr, Nd). Geosci. Front. https://doi.org/10.1016/j.gsf.2020.03.015.
Wilson, M., 1989. Igneous Petrogenesis: A Global Tectonic Approach. Unwin Hyman, London.
Workman, R.K., Hart, S.R., 2005. Major and trace element composition of the depleted MORB mantle (DMM). Earth Planet. Sci. Lett. 231, 53–72.
Zindler, A., Hart, S.R., 1986. Chemical geodynamics. Annu. Rev. Earth Planet. Sci. 14, 493–571.